

eScholarship@UMassChan

Exploring the Phenomenon of MNNG Dose-Dependent Death Polypharmacology

Item Type	Master's Thesis
Authors	Fontana, Rachel
DOI	10.13028/dmby-d122
Publisher	UMass Chan Medical School
Rights	Copyright © 2023 Fontana
Download date	2026-05-08 08:50:46
Item License	https://creativecommons.org/licenses/by/4.0/
Link to Item	https://hdl.handle.net/20.500.14038/51826

**EXPLORING THE PHENOMENON OF MNNG DOSE-DEPENDENT DEATH
POLYPHARMACOLOGY**

A Master's Thesis Presented

By

Rachel Fontana

Submitted to the Faculty of the
Morningside Graduate School of Biomedical Sciences at UMass Chan Medical
School in partial fulfillment of the requirements for the degree of

MASTER OF SCIENCE

February 23, 2023

Bioinformatics and Integrative Biology, Systems Biology

**EXPLORING THE PHENOMENON OF MNNG DOSE-DEPENDENT DEATH
POLYPHARMACOLOGY**

A Master's Thesis Presented

By

Rachel Fontana

The signatures of the Master's Thesis Committee signify completion and approval as to style and content of the Thesis

Sharon Cantor, Ph.D., Chair of Committee

Michelle Kelliher, Ph.D., Member of Committee

Amir Mitchell, Ph.D., Member of Committee

The signature of the Dean of the Graduate School of Biomedical Sciences signifies that the student has met all master's degree graduation requirements of the school.

Mary Ellen Lane, Ph.D.,
Dean of the Graduate School of Biomedical Sciences

Bioinformatics and Integrative Biology, Systems Biology

February 23, 2023

ACKNOWLEDGEMENTS

Foremost, I would like to thank my thesis advisor, Dr. Michael Lee, for his mentorship and guidance. Our conversations really helped to shape this project and my mindset as a scientist.

Importantly, I would also like to thank my Lee Lab members (past and present) for their amazing support both academically and personally. Specifically, I would like to thank Megan Honeywell, Nicholas Harper, Gavin Birdsall, Hannah Schwartz, and Anitha Rajendran for their help in shaping this project. Thank you for all of the conversations, scientific advice, and experimental troubleshooting.

Moreover, I would like to thank my TRAC and MS committees: Dr. Sharon Cantor, Dr. Marian Walhout, Dr. Michelle Kelliher, and Dr. Amir Mitchell. Their assistance was invaluable for this project and for my personal development.

Finally, I would like to thank my family, friends, and loved ones for their unending support and encouragement for all that I do. I am so lucky to have you all in my life. Specifically, I would like to thank Derek Chu, Richard Fontana, Mary Fontana, Katie Meier, and Gloria Fontana for their love and assistance.

Thank you all.

ABSTRACT

Regulated cell death (RCD) is composed of several pathways that control cell fate. While each pathway is mechanistically distinct, these pathways have been shown to interact. Most of these interactions tend to be antagonistic, such that activation of one pathway blocks the subsequent activation of another pathway. This highlights that death pathways tend to be mutually exclusive. Thus, combining two cytotoxic drugs that activate different death pathways could result in less cell death than predicted, hampering therapeutic efficacy. As such, it is necessary to characterize which death pathways are activated by clinically relevant drugs, particularly for drug combination studies. However, studies of death pathway engagement are complicated by the fact that many drugs are capable of activating multiple RCD pathways. In order to improve annotations of RCD pathway activation by specific stimuli, we need to learn what features dictate which death pathway is activated.

To study this phenomenon, we focused on characterizing RCD execution after treatment with methylnitrosoguanidine (MNNG), a DNA alkylating agent. MNNG is the canonical activator of parthanatos, an inflammatory form of RCD dependent on PARP-1 hyper-activation. We found that MNNG exhibits dose-dependent changes in death features, such as death onset time and death rate, indicative of a death mechanism change. As such **we hypothesized that MNNG can induce multiple RCD pathways in a dose-dependent fashion.** We found

that this dose-dependent change in death features was generalizable to multiple cell lines. Moreover, we established that the phenotype was not due to PARP-trapping effects. Importantly, we uncovered that MNNG does induce a death mechanism switch. We found that MNNG is capable of inducing either parthanatos or apoptosis, depending on the dose. We also found evidence that the two death pathways induced by MNNG were mutually exclusive. And lastly, we established that the death mechanism switch was not due to altered mismatch repair (MMR). The information from this study could help to shed light on clinical outcomes from drug combination trials, specifically combinations with DNA damaging agents and PARP inhibitors.

TABLE OF CONTENTS

Acknowledgements	i
Abstract	ii
Table of Contents	iv
List of Tables	vii
List of Figures	viii
List of Symbols and Abbreviations	ix
Preface	xii
CHAPTER I: Introduction	1
1.1 Cancer Cell Evasion of Apoptosis	1
1.2 Alternate Death Pathways to Target Cancer	6
1.3 Parthanatos, an Under-explored Death Pathway	8
1.4 RCD Interactions and Rational Drug Combination Design	11
1.5 Clinical Importance of Death Polypharmacology	13
1.6 Measuring Cancer Cell Death	15
1.7 Thesis Overview	20
CHAPTER II: MNNG Exhibits Dose-dependent Death Polypharmacology	21
2.1 Introduction	21
2.2 Results	25
2.2A <i>MNNG exhibits dose-dependent changes in death onset time and death rate, indicative of a death mechanism change</i>	25

2.2B MNNG dose-dependent death mechanism switch is generalizable	30
2.2C MNNG dose-dependent death mechanism switch is not due to PARP-trapping effects	33
2.2D MNNG exhibits death polypharmacology, capable of inducing either parthanatos or apoptosis	36
2.2E: MNNG-induced parthanatos and apoptosis are mutually exclusive	42
2.2F MNNG death polypharmacology is not due to altered MMR response	47
2.3 Discussion	51
2.4 Materials and Methods	55
2.4A: Cell lines	55
2.4B: General reagents	57
2.4C: BAK/BAX-DKO U2OS and PARP1-KO U2OS cell line generation	57
2.4D: FLICK assay	58
2.4E: Cell Titer Glo	59
2.4F: STACK assay	60
2.4G: Western blot	61
2.4H: Flow cytometry co-culture assay	63
2.4I: Data analysis	64
CHAPTER III: Discussion	65
3.1 Death Polypharmacology Considerations for Cancer Therapies	65
3.2 Implications for Combinations of DNA Damaging Agents and PARP Inhibitors	69

3.3 Importance of Kinetics for Capturing Death Polypharmacology	70
3.4 Improving Mechanistic Insight for the Parthanatos Pathway	72
Bibliography	76

LIST OF TABLES

<u>Table 2.1</u> List of RCD pathway inhibitors	37
---	----

LIST OF FIGURES

<u>Figure 1.1</u> Intrinsic apoptosis pathway	5
<u>Figure 1.2</u> Parthanatos pathway	10
<u>Figure 1.3</u> Drug response metrics	19
<u>Figure 2.1</u> MNNG exhibits dose-dependent changes in death onset time and death rate, indicative of a death mechanism change	29
<u>Figure 2.2</u> MNNG dose-dependent death mechanism switch is generalizable	32
<u>Figure 2.3</u> MNNG dose-dependent death mechanism switch is not due to PARP-trapping effects	35
<u>Figure 2.4</u> MNNG exhibits dose-dependent death polypharmacology, capable of parthanatos or apoptosis	41
<u>Figure 2.5</u> MNNG-induced parthanatos and apoptosis are mutually exclusive	46
<u>Figure 2.6</u> MNNG death polypharmacology is not due to altered MMR response	50

LIST OF SYMBOLS AND ABBREVIATIONS

- ACD – accidental cell death
- AIF – apoptosis-inducing factor
- APC – allophycocyanin
- ATP – adenosine triphosphate
- APAF1 – apoptotic peptidase activating factor 1
- AUC – area under the curve
- BAK – BCL-2-homologous antagonist killer
- BAX – BCL-2-associated X protein
- BCL-1 – B-cell lymphoma 1 protein
- BCL-2 – B-cell lymphoma 2 protein
- BCL-X_L – B-cell lymphoma extra-large protein
- β -GP – beta-glycerophosphate
- DDR – DNA damage response
- DKO – double knockout
- DMEM – Dulbecco's Modified Eagle Medium
- DNA – deoxyribonucleic acid
- EDTA – ethylenediaminetetraacetic
- FBS – fetal bovine serum
- Ferrostatin-1 – synthetic antioxidant (ferroptosis inhibitor)

- FLICK – fluorescence-based and lysis-dependent inference of cell death kinetics
- FV – fractional viability
- GR – growth rate inhibition
- KO – knockout
- LED – lag exponential death
- LF – lethal fraction
- MIF – macrophage migration inhibition factor
- MLKL – mixed lineage kinase domain like pseudokinase
- MNNG – methylnitrosoguanidine
- MMP – mitochondria membrane potential
- MMR – mismatch repair
- MOMP – mitochondrial outer membrane permeabilization
- NAD – nicotinamide adenine dinucleotide
- NAF – sodium fluoride
- Na_3VO_4 – sodium orthovanadate
- NCCD – nomenclature committee on cell death
- Necrostatin-1 – RIPK1 inhibitor (necroptosis inhibitor)
- PAR – poly ADP-ribose
- PARG – poly ADP-ribose glycohydrolase
- PARP-1 – poly (ADP-ribose) polymerase 1
- PBS – phosphate buffered saline

- PBST – phosphate buffered saline with 0.1% tween
- PCD – programmed cell death
- PMSF – phenylmethanesulphonyl fluoride
- RIPK1 – receptor-interacting serine/threonine-protein kinase 1
- RIPK3 – receptor-interacting serine/threonine-protein kinase 3
- RCD – regulated cell death
- ROS – reactive oxygen species
- RT – room temperature
- Rucaparib – PARP-1 inhibitor (parthanatos inhibitor)
- RV – relative viability
- SDS – sodium dodecyl sulfate
- SMAC – second mitochondria-derived activator of caspase protein
- STACK – scalable time-lapse analysis of cell death
- TNF α – tumor necrosis factor alpha
- TNFR1 – tumor necrosis factor receptor 1
- Tris-HCl – tris hydrochloride
- VX-765 – selective inhibitor of Caspase-1 (pyroptosis inhibitor)
- WT – wild type
- XIAP – X-linked inhibitor of apoptosis protein
- Z-IETD-FMK – selective inhibitor of Caspase-8 (extrinsic apoptosis inhibitor)
- Z-VAD-FMK – pan-caspase inhibitor (apoptosis inhibitor)

PREFACE

Reagent generation: MMR-proficient and MMR-deficient cell lines were generous gifts from the from the S. Cantor Lab (UMass Chan Medical School). These cell lines were used in previous studies listed below:

Gupta D, Lin B, Cowan A, and Heinen CD. ATR-Chk1 activation mitigates replication stress caused by mismatch repair-dependent processing of DNA damage. *PNAS*. **115(7)**, 1523-1528 (2018).

Peng M, Xie J, Ucher A, Stavnezer J, and Cantor SB. Crosstalk between BRCA-Fanconi anemia and mismatch repair pathways prevent MSH2-dependent aberrant DNA damage responses. *EMBO*. **33(15)**, 1698-1712 (2014).

BAK/BAX-DKO U2OS were developed by Dr. Ryan Richards in the Lee Lab. These cell lines were used in previous studies listed below:

Richards R, Schwartz HR, Honeywell ME, Stewart MS, Cruz-Gordillo P, Joyce AJ, Landry BD, and Lee MJ. Drug antagonism and single-agent dominance result from differences in death kinetics. *Nat Chem Bio*. **16**, 791-800 (2020).

PARP-1-KO U2OS were developed by Yuqing Wang in the Lee Lab.

Author contributions: This project was conceived by Dr. Michael Lee, Rachel Fontana, and Dr. Anitha Rajendran. All experiments and data analysis were performed by Rachel Fontana. Curve fitting, LED modeling, and GR modeling were functions developed by Dr. Michael Lee and Dr. Ryan Richards. These functions are posted on the Lee Lab GitHub page.

Figure creation: Several figures were *created with BioRender.com*. Figures created with BioRender.com are noted in the figure legend.

CHAPTER I: INTRODUCTION

1.1 Cancer Cell Evasion of Apoptosis

Apoptosis is the most-studied form of RCD (regulated cell death) and one of the most-studied pathways of all time.^{1,2} It plays key roles in development, allowing for elimination of specific cells or remodeling of organs.¹ It is also important for organism homeostasis, allowing for cell turnover.^{1,2} Importantly, apoptosis is also relevant to the pathogenesis of many diseases, such as cancer, heart disease, and neurological disorders.¹

Apoptosis can be extrinsic or intrinsic. Extrinsic apoptosis occurs when a cell encounters an extracellular apoptotic stimulus, such as $\text{TNF}\alpha$.^{2,3} Conversely, intrinsic apoptosis occurs when a cell experiences an intracellular apoptotic stimulus, such as DNA damage, reactive oxygen species (ROS), or endoplasmic reticulum (ER) stress (Fig 1.1).^{2,4} Upon receipt of an intrinsic apoptotic stimulus, cells activate pro-apoptotic BH3-only proteins.² In turn, BH3-only proteins induce BAK and BAX oligomerization, which produce pores in the mitochondria.² Both the BH3-only proteins and BAK/BAX oligomerization can be inhibited by the anti-apoptotic BCL-family proteins, BCL-2, BCL-X_L, and MCL-1.²

BAK/BAX pore formation ultimately induces mitochondrial outer membrane permeabilization (MOMP) (Fig 1.1).^{2,5,6,7,8} This leads to the release of pro-apoptotic factors, SMAC and cytochrome C.^{2,9,10,11,12,13,14} SMAC release leads to inhibition of anti-apoptotic factor X-linked inhibitor of apoptosis (XIAP).^{2,13,14} If XIAP is not inhibited, XIAP prevents apoptosis by blocking downstream caspase activity.^{2,15} Released cytochrome C interacts with apoptotic peptidase activating factor 1 (APAF1) and pro-Caspase-9 to form the apoptosome. The formation of this structure leads to Caspase-9 activation.^{2,11} In turn, active Caspase-9 cleaves, and subsequently activates, Caspase-7 and Caspase-3. These caspases serve as the executioners of apoptosis, causing the downstream events that ultimately result in apoptotic death.²

A key feature of apoptosis is the production of a cell corpse that induces little-to-no immunogenicity.² To accomplish this, the executioner caspases induce DNA fragmentation.² Cell-free DNA can stimulate the immune system; thus, DNA degradation limits immune response.² Moreover, the executioner caspases induce the formation of apoptotic bodies that express phosphatidylserine (PS).^{2,16,17,18,19} This facilitates corpse clearance by phagocytes, which also limits immune response.² These morphological features distinguish both intrinsic and extrinsic apoptosis from other forms of RCD, which frequently produce immunogenic cell corpses. As such, apoptosis is generally considered to be a 'silent' form of cell death.² The interplay of RCD execution and immune system engagement can have important ramifications for clinical drug treatments, especially in cancer.

Cancer is a disease of dysregulated apoptosis.¹ Over the course of cancer development, cancer cells frequently experience the stress signals that initiate apoptosis, such as increased ROS and DNA damage.^{20,21} As such, cancer cells have developed various means of evading apoptotic death.^{21,22} Foremost, cancer cells can evade apoptosis through an imbalance of pro-apoptotic and anti-apoptotic proteins.¹ Cancer cells can upregulate anti-apoptotic BCL-family proteins. Overexpression or amplification of BCL-family proteins is observed in many cancer types and causes increased resistance to cancer therapeutics.^{20,23,24,25,26,27,28,29,30,31,32} Cancer cells can also evade apoptosis by stabilizing anti-apoptotic proteins, such as MCL-1.^{20,33,34,35,36}

Alternately, cancer cells can evade apoptosis through downregulation of pro-apoptotic proteins. Loss of expression of the pro-apoptotic protein APAF1 has been reported in many cancer types.^{20,37,38,39,40,41,42,43,44} Moreover, increased turnover of the pro-apoptotic protein BAX has been shown to lead to worse clinical outcomes in cancer patients.^{20,45} Cancer cells can also evade apoptosis through a reduction in caspase function.¹ Downregulation of caspases is associated with increased instances of cancer and worse clinical outcomes in cancer patients.^{1,46,47,48}

Cancer evasion of apoptosis clearly has important ramifications for clinical treatment strategies. Many of the frequently used clinical chemotherapies induce apoptosis. This includes key agents such as Docetaxel, Etoposide, Paclitaxel, Temozolomide, Topotecan, Vinblastine, and Vincristine.⁴⁹ Due to cancer evasion

of apoptosis, it is unsurprising why many cancers are resistant to treatment with these apoptotic chemotherapies. As such, this highlights the importance of studying and developing non-apoptotic cancer therapies as alternate treatment strategies. However, to accomplish such an endeavor, it is first necessary to improve our knowledge and mechanistic insight into alternate forms of RCD. Currently, many non-apoptotic RCD pathways are poorly defined.

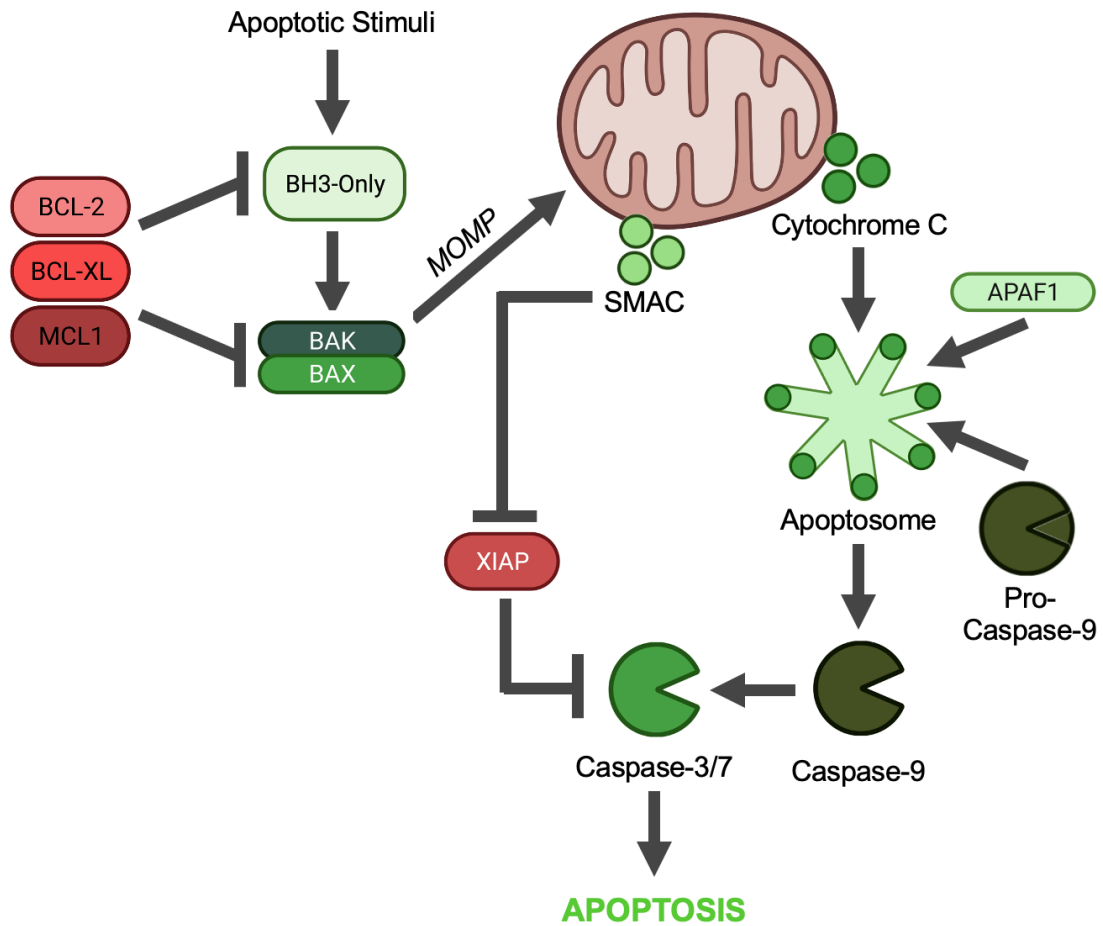


FIGURE 1.1 Intrinsic apoptosis pathway. Apoptosis occurs when an apoptotic stimulus activates BH3-only proteins, which in turn induce BAK/BAX protein oligomerization. This then causes pore formation and MOMP, which results in release of SMAC and cytochrome C. Cytochrome C interacts with APAF1 and pro-Caspase-9, resulting in the formation of the apoptosome. This causes Caspase-9 activation, which results in downstream Caspase-7 and Caspase-3 activation. Activation of these downstream caspases allows for execution of apoptosis. Apoptosis can be inhibited by anti-apoptotic BCL-family proteins (BCL-2, BCL-XL, and MCL1). Apoptosis can also be inhibited by XIAP. Imbalances in these proteins can result in dysregulation of apoptosis, such as cancer apoptosis evasion. *Created with BioRender.com.*

1.2 Alternate Death Pathways to Target Cancer

Cells die through accidental cell death (ACD) or regulated cell death (RCD). ACD occurs when cells experience a critical physical, chemical, or mechanical insult that is unregulatable and causes instantaneous death.² Conversely, RCD requires the use of specific molecular machinery and signaling cascades to execute death.² As the name suggests, RCD is regulatable. Programmed cell death (PCD) subroutines are included under RCD.² PCD only occurs due to death activation with internal stimuli. Examples of PCD include tissue turnover and coordinated death during organism development.² Alternately, RCD occurs due to death activation with internal or external stimuli.² As such, most clinical cytotoxic cancer therapies induce cell death via RCD engagement.

RCD is composed of several distinct pathways that control cell fate. Currently, the Nomenclature Committee on Cell Death (NCCD) defines 12 pathways under RCD.² These pathways can be differentiated and defined based on the molecular machinery, morphologies, and immunological effects that occur upon cell death. For instance, RCD pathways are typically characterized as having either apoptotic or necrotic death morphologies. Apoptotic death morphologies are associated with less immunogenic death pathways, such as intrinsic apoptosis and extrinsic apoptosis. Conversely, necrotic death morphologies are associated with more immunogenic death pathways, such as pyroptosis, necroptosis, ferroptosis, and

parthanatos.² The interplay of RCD execution and immune system engagement can have important ramifications for clinical cancer treatments.

Many of these immunogenic, non-apoptotic death pathways have been implicated as potential targets for cancer therapies. For instance, much research in recent years has focused on targeting ferroptosis as a compelling cancer therapy. This interest is in part due to ferroptosis being so mechanistically distinct from apoptosis.⁵⁰ Unlike apoptotic death, ferroptotic death does not involve caspases. Instead, ferroptosis occurs due to an imbalance in lipid peroxides. This imbalance in lipids peroxides can be driven by increased reactive oxygen species (ROS), which is a common characteristic of cancer.⁵⁰

Another attractive death pathway for treating cancer is parthanatos.⁵¹ Like ferroptosis, parthanatos is another caspase-independent form of death. Parthanatos is an inflammatory form of RCD dependent upon poly (ADP-ribose) polymerase 1 (PARP-1) hyper-activation.^{2,3} However, the precise mechanism of parthanatos is poorly defined, making it challenging to develop parthanatotic therapies for targeting cancer. As such, to design novel non-apoptotic cancer therapies, it is necessary to improve our current understanding of non-apoptotic RCD pathways.

1.3 Parthanatos, an Under-explored Death Pathway

The term parthanatos was coined in 2006 to describe a new form of cell death that was distinct from apoptosis or necrosis.^{52,53} Since its discovery, minimal progress has been made in uncovering the specific molecular determinants of parthanatotic death. All studies agree that parthanatos involves DNA repair protein poly (ADP-ribose) polymerase 1 (PARP-1) (Fig 1.2).^{51,54,55,56,57,58,59} DNA damage, specifically DNA breaks, can lead to PARP-1 hyper-activation.^{51,54,55,56,57,58,59} Upon PARP-1 hyper-activation, PARP-1 produces poly ADP-ribose (PAR) polymers, which can attach to various proteins, such as PARP-1, histones, and other DNA repair proteins.^{54,55,59} PAR polymers can vary in complexity and length.⁶⁰ More complex and longer PAR polymers are more likely to induce death.⁶⁰ Moreover, production of PAR polymers results in depletion of NAD pools and ATP pools.⁵¹ Depletion of these molecules has also been implicated to play a role in the execution of parthanatos.⁵¹ Importantly, degradation of PAR polymers by poly ADP-ribose glycohydrolase (PARG) leads to the inhibition parthanatos.⁶⁰

After PAR production and subsequent PAR accumulation, the cell experiences loss of mitochondria membrane potential (MMP) and eventually undergoes death (Fig 1.2).^{59,60} However, the exact steps in this process are unclear. Some studies suggest a model involving apoptosis-inducing factor (AIF). In this model, PAR release from the nucleus is anticipated to trigger AIF release from the

mitochondria.^{54,55} This process occurs through some unknown mechanism. It has been proposed that PAR binds to an unknown protein factor, which is responsible for trafficking PAR to the mitochondria.⁵⁶ Once in the mitochondria, PAR is thought to stimulate AIF release.⁵⁶ Upon, AIF release, AIF is thought to interact with macrophage migration inhibition factor (MIF). This AIF-MIF complex is trafficked to the nucleus, where it induces DNA degradation and subsequent parthanatotic death.⁵⁶

This AIF model of parthanatos has several shortcomings. Foremost, no studies to-date have been able to define how PAR triggers AIF release from the mitochondria. Additionally, many alternate studies have shown that parthanatos can occur independently of AIF.^{61,62,63} As such it is unclear whether the proposed AIF model of parthanatos is generalizable across a broad range of genetic backgrounds, or specific to a limited set of cell types and experimental conditions. Regardless, this uncertainty highlights the need for additional studies into the mechanism of parthanatos. Specifically, additional pathway clarity is required to develop parthanatotic therapies to target cancer.

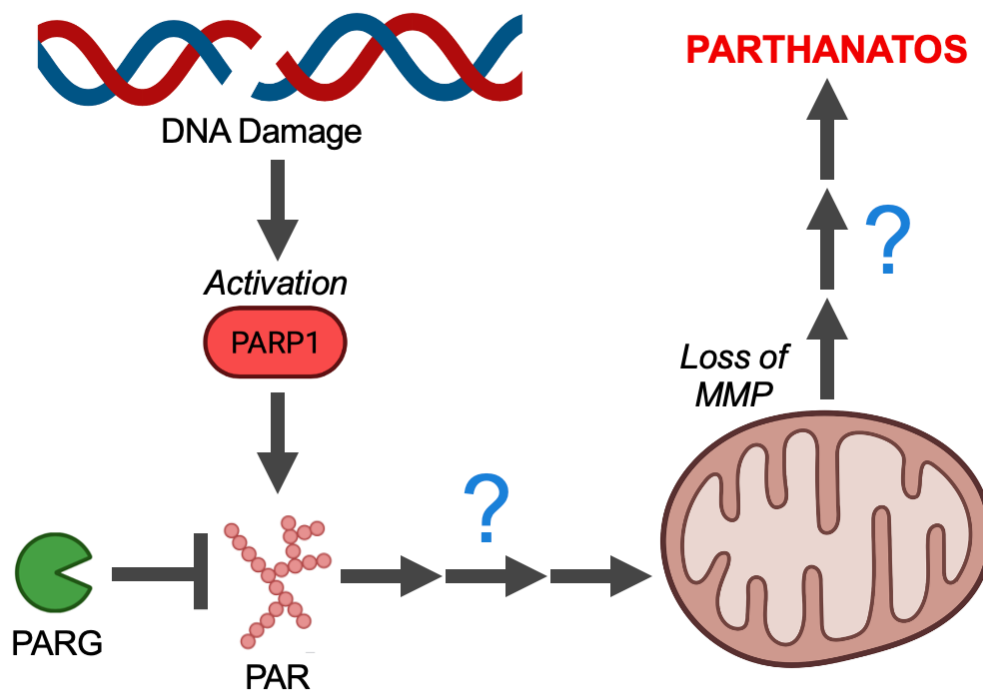


FIGURE 1.2 Parthanatos pathway. DNA damage can induce PARP-1 activation. PARP-1 hyper-activation results in PAR production, which can be inhibited by PARG. Accumulation of PAR ultimately causes MMP and downstream parthanatotic death execution. However, the exact steps in this process are currently unclear. *Created with BioRender.com.*

1.4 RCD Interactions and Rational Drug Combination Design

RCD is composed of multiple death pathways. While each death pathway is distinct, with unique mechanisms of signal propagation, execution, and physiological consequences, interactions between death pathways are known to exist.² A recent study from our group, Richards *et al* (2020), found a dense network of positive and negative interactions between death pathways.⁴⁹ These interactions were strongly enriched for antagonism, which was attributed to inhibitory crosstalk between death pathways.⁴⁹

This study specifically highlighted the mutual exclusivity of intrinsic apoptosis and parthanatos.⁴⁹ Administering an apoptotic drug and a parthanatotic drug concurrently resulted in less markers of activation for each death pathway than expected.⁴⁹ Apoptotic inhibition of parthanatos was unsurprising. Apoptotic executioner Caspase-3 cleaves PARP-1, rendering it inactive.⁶⁴ Inactive PARP-1 is incapable of initiating parthanatos. Thus, apoptosis can block parthanatos. However, this study also found that parthanatos can inhibit apoptosis.⁴⁹ Parthanatotic inhibition of apoptosis was very surprising. As we currently understand parthanatos, it is unclear how this pathway would be capable of inhibiting apoptosis. This suggests that additional studies of parthanatos are required to elucidate this antagonistic RCD pathway interaction.

Antagonistic death pathway interactions also occur between extrinsic apoptosis and necroptosis.⁶⁵ Both pathways can be induced by TNF α interaction with TNFR1. Activation of TNFR1 can lead to activation of Caspase-8, which is required for execution of extrinsic apoptosis.^{2,3} Activation of TNFR1 can also activate RIPK1, RIPK3, and MLKL, which are required for necroptosis.^{2,3} However, Caspase-8 inhibits RIPK3. Thus, necroptosis can only proceed when Caspase-8, the executioner of extrinsic apoptosis, is inhibited.⁶⁵ As such, activation of extrinsic apoptosis is antagonistic for activation of necroptosis.

The prevalence of antagonistic death pathway interactions is of utmost importance for clinical treatment strategies. Most cancer treatments rely on drug combination therapies.⁶⁶ These combinations could include chemotherapies that induce different RCD pathways. A naïve assumption is that drug combination of two lethal agents will produce increased cytotoxicity. However, if the two lethal agents induce antagonistic death pathways, the drug combination could produce less cytotoxicity than expected. As such, one cannot presume that the combination of two cytotoxic drugs will produce more death than either drug on its own. Therefore, to create rational drug combinations for clinical use, it is necessary to fully characterize how each drug induces death. Moreover, to create rational drug combinations, it is also essential to fully characterize RCD pathway interactions.

1.5 Clinical Importance of Death Polypharmacology

Polypharmacology occurs when a single drug interacts with multiple targets. In the context of cell death, this would occur when a single drug induces multiple RCD pathways. To describe this phenomenon, we will coin the term, 'death polypharmacology'. Such death polypharmacology is currently understudied. Death polypharmacology could occur through several mechanisms, outlined below.

First, death polypharmacology could occur due to a lack of drug-specificity. In this situation, a single drug would turn on multiple RCD pathways, independent of drug dose and independent of genetic context. This likely occurs with 'dirty' drugs. Many drugs are 'dirty', a term for drugs that bind non-specifically to multiple drug targets.⁶⁷ Due to hitting multiple targets, 'dirty' drugs may be capable of initiating multiple RCD pathways in parallel. Although 'dirty' drugs increase the chance of toxicity and adverse events, they are also useful for treating complex diseases, like cancer.⁶⁷ In fact, 'dirty' drugs, such as Axitinib, Sunitinib, and Sorafenib, function as FDA-approved cancer treatments.⁶⁷ The 'dirty' clinical agent Sorafenib has been shown to exhibit death polypharmacology. Sorafenib can induce both ferroptosis and apoptosis.^{2,68,69,70,71,72} Overall, this phenomenon is currently not well-documented. This type of non-specific death polypharmacology is important to note though since it could impact drug outcomes in the clinic. However, this non-

specific death polypharmacology cannot be controlled since it is not a tunable phenomenon.

Second, death polypharmacology could also occur due to genetic context. In this situation, a single drug would induce a different RCD pathway dependent on cell type, but independent of drug dose. Such genetic-dependent death polypharmacology has been documented. The clinical agent Doxorubicin is known to induce apoptosis.⁷³ Yet, in some genetic contexts Doxorubicin can induce necroptosis instead.⁷⁴ This highlights that genetic context can alter drug death pathway induction. Again, although instances have been documented, it still remains a poorly studied phenomenon. Genetic-dependent death polypharmacology is important to note though since it could impact clinical drug outcomes. However, genetic-dependent death polypharmacology cannot be controlled. It can only be used as a biomarker tool to influence which genetic diseases will benefit from the drug.

And finally, death polypharmacology could also occur through dose-dependence. In this scenario, a single drug would induce a different RCD pathway dependent upon drug dose, but independent of genetic context. This type of death polypharmacology is important to record since it could impact drug outcomes. Notably, unlike the other two previously described mechanisms, dose-dependent death polypharmacology can be controlled since it is a tunable phenomenon. Altering the dose, would alter which death pathway is induced. As such, dose-

dependent death polypharmacology could have immense clinical utility. However, to our knowledge, such situations are currently not documented.

As alluded to, studying the phenomenon of death polypharmacology is important for clinical therapies. Death pathways play an important role in clinical outcomes. In some disease states it may be advantageous to induce non-immunogenic, apoptotic death. However, in other disease states it may be advantageous to induce immunogenic, non-apoptotic death. Moreover, in the context of drug combinations of cytotoxic agents, it is necessary to carefully characterize which RCD pathway is induced by each agent. This is due to the prevalence of antagonistic interactions between RCD pathways.⁴⁹ Antagonistic combinations of cytotoxic agents would result in less cell death than expected. This could be detrimental for clinical therapy outcomes in the context of cancer. As such, fully understanding what form of RCD will be induced at a given drug dose in a given genetic context is necessary to predict clinical outcomes. For this reason, studying death polypharmacology is necessary for clinical agents.

1.6 Measuring Cell Death

In order to fully characterize a drug's ability to induce a specific death pathway, it is necessary to measure cell death. However, traditional pharmacological assays frequently fail to measure cell death. These assays instead make use of relative

viability (RV) metrics. RV is the comparison of the number of live drug-treated cells to the number of live vehicle-treated cells (Fig 1.3).⁷⁵ As such, RV cannot parse growth arrest from cell death. RV metrics are frequently derived from assays such as Cell Titer Glo, MTT, and colony formation assays.⁷⁶ These assays are common in many drug characterization studies due to their ease of use.

GR (growth rate inhibition) is another metric used for evaluating drug response through the number of live cells.^{77,78} GR is the comparison of drug-treated cell growth rates and vehicle-treated cell growth rates. By comparing the growth rates, GR predicts whether the cell population is experiencing growth arrest or cell death. GR values less than one, but greater than zero, indicate partial growth arrest. GR values less than zero indicate cell death. However, to make this prediction, GR expects that a cell population can either experience growth arrest or cell death. Our lab has found that this expectation is incorrect. Within a population of cells, it is possible for some cells to experience growth arrest at the same time as other cells experience death.⁷⁶

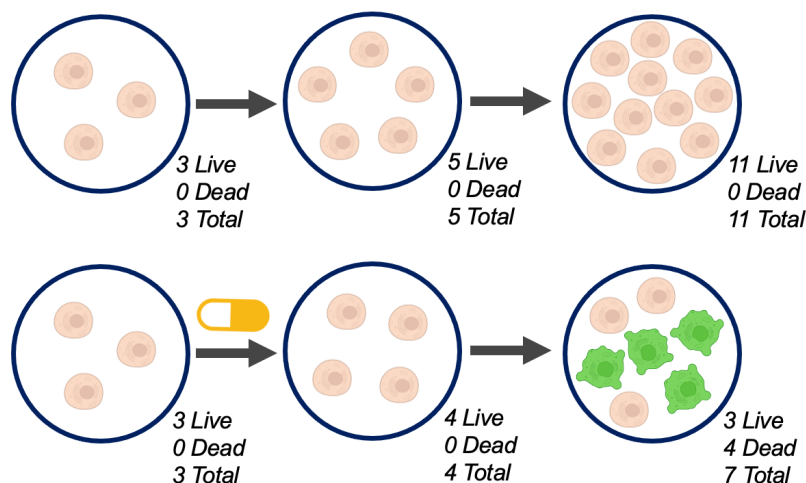
As such, it is necessary to rely on assays that directly measure death. Fractional viability (FV) is the comparison of the number of live drug-treated cells to the number of total (live and dead) drug-treated cells (Fig 1.3). FV metrics can be derived from assays such as fluorescence-based and lysis-dependent inference of cell death kinetics (FLICK) and scalable time-lapse analysis of cell death (STACK).^{75,79} FLICK is a live cell plate-reader assay, whereas STACK is a live cell microscopy assay. Both of these assays rely on the use of sytox, a live cell

impermeant dye that fluoresces upon binding DNA.⁷⁵ Because sytox fluorescence is only dependent upon membrane breakdown, sytox can be used to measure death independently of the death mechanism.⁷⁵ This is powerful, since many other forms of death measurement assays rely on RCD pathway specific metrics, such as Annexin V staining, which only scores apoptotic death.⁸⁰

Both FLICK and STACK allow for the direct measurement of dead cells across time. STACK also allows for the direct measurement of total cells across time. In STACK, cells are labeled prior to the start of the experiment to monitor changes in total cells across time.⁷⁹ FLICK allows for the inferred measurement of total cells across time.⁷⁵ Cells are lysed at the end of the assay to generate the ending number of total cells. Additionally, a mock plate of cells is lysed at the start of the assay to generate the starting number of total cells. By fitting the starting and ending number of total cells to an exponential curve, it is possible to back-calculate the expected number of total cells at each timepoint.⁷⁵

Since both FLICK and STACK monitor live and dead cell numbers across time, they can be used to generate LF (lethal fraction) kinetics. LF is the comparison of the number of dead drug-treated cells to the number of total (live and dead) drug-treated cells (Fig 1.3). LF data is plotted for a single dose across time and fit to a lag-exponential model of cell death (LED).⁷⁵ The resulting plot allows for inference of features such as death onset time and death rate. Changes in these kinetic death features are indicative of changes in death mechanism. Thus, comparing

changes in these kinetic death features, across dose and genetic background, allows us to capture instances of potential death polypharmacology.



$$RV_{\text{end}} = \frac{\# \text{ Live Drug-Treated}}{\# \text{ Live Untreated}} = \frac{3}{11} = 27\%$$

$$FV_{\text{end}} = \frac{\# \text{ Live Drug-Treated}}{\# \text{ Total Drug-Treated}} = \frac{3}{7} = 43\%$$

$$LF_{\text{end}} = \frac{\# \text{ Dead Drug-Treated}}{\# \text{ Total Drug-Treated}} = \frac{4}{7} = 57\%$$

FIGURE 1.3 Drug response metrics. Drug response assays focus on either live, dead, or total cells numbers. Relative viability (RV) compares the number of live cells in a drug-treated condition to the number of live cells in an untreated (or vehicle-treated) condition. As such, RV only requires the measurement of live cells. RV highlights how the drug-treated population changes relative to the un-treated population. Fractional viability (FV) compares the number of live cells to the number of total cells within the same drug-treated condition. As such, FV requires the measurement of dead and total cell numbers. Live cell numbers can be extrapolated. Lethal fraction (LF) compares the number of dead cells to the number of total cells within the same drug-treated condition. As such, LF requires the measurement of dead and total cell numbers. Comparing these metrics at endpoint allows for an integrated view of growth-arrest and cell-death. Looking at these metrics across time provides even more insight on drug-response. In this example, by capturing live and dead cell numbers over time, it is apparent that the drug induces growth-arrest prior to cell-death. *Created with BioRender.com.*

1.7 Thesis Overview

Many common clinical cancer therapies make use of apoptotic agents.⁴⁹ Unfortunately, many cancers have undertaken steps to evade apoptotic death.¹ This is one mechanism by which cancers experience drug resistance. As such it is necessary to explore drugs that induce alternate RCD pathways as cancer therapeutics. However, incorporation of non-apoptotic drugs into clinical treatment strategies could pose new challenges. Foremost, many clinical strategies involve drug combinations.⁶⁶ Combining drugs of different RCD pathways most frequently leads to antagonism,⁴⁹ which would likely be clinically disadvantageous. As such it would be necessary to carefully annotate what death pathways are induced by what drugs. This is not a trivial challenge though, due to the expected existence of death polypharmacology. Death polypharmacology remains a poorly explored concept. As such, this thesis will be focused on characterizing a specific instance of dose-dependent death polypharmacology observed with the DNA alkylating agent MNNG.

CHAPTER II: MNNG EXHIBITS DOSE-DEPENDENT DEATH POLYPHARMACOLOGY

2.1 Introduction

Regulated cell death (RCD) is comprised of multiple pathways that control cell fate. While each pathway is mechanistically distinct, these pathways have been shown to interact. Most of these RCD pathway interactions are antagonistic.⁴⁹ Activation of one death pathway blocks the subsequent activation of another death pathway.⁴⁹ As such, death pathway antagonism tends to be mutually exclusive. This has important implications for clinical drug combination strategies in cancer treatment. Combining cytotoxic drugs that activate different death pathways could result in less cell death than expected. This would hamper drug combination clinical outcomes. As such, it is necessary to characterize which death pathways are activated by clinically relevant drugs, particularly for drug combination studies. However, studies of death pathway engagement are complicated by the fact that many drugs are capable of death polypharmacology. Death polypharmacology occurs when a drug can activate multiple RCD pathways. Therefore, in order to improve annotations of RCD pathway activation by specific stimuli, we need to learn what features dictate which death pathway is activated.

As such, we focused on characterizing RCD pathway engagement of methylnitronitrosoguanidine (MNNG), a DNA alkylating agent. MNNG is the canonical activator of parthanatos, an inflammatory form of RCD dependent on PARP-1 hyper-activation. In this study, we found that MNNG displays dose-dependent changes in key features of death, indicative of a death mechanism switch. Low doses of MNNG induce no death. Intermediate doses of MNNG induce death with a faster onset time but slower rate. Conversely, high doses of MNNG induce death with a slower onset time but faster rate. The observed dose-dependent change in death onset time and death rate was indicative of a death mechanism switch.

To confirm that a death mechanism switch had occurred, we tested MNNG plus Rucaparib, the inhibitor of parthanatos. Importantly, we found that Rucaparib was only capable of blocking death at intermediate doses of MNNG. Rucaparib instead exacerbated death at high doses of MNNG. Thus, intermediate MNNG doses induced parthanatotic death, whereas high MNNG doses induced non-parthanatotic death. Together, this data suggested that a dose-dependent death mechanism switch had occurred.

We found that the MNNG dose-dependent death mechanism switch was generalizable. Out of a panel of cell lines of varied genetic backgrounds, we noticed that other cell types also displayed this phenotype. Although we found the phenotype was generalizable, we were concerned that it might be due to an artifact. The parthanatotic inhibitor, Rucaparib, inhibits PARP-1 by trapping it on

DNA. PARP-trapping has been suggested to increase DNA damage, leading to increased cell death.^{81,82} As such, we were concerned that the phenotype observed at high doses of MNNG was due to PARP-trapping rather than PARP-1-inhibition. However, PARP-1-KO cells also displayed exacerbated death at high doses of MNNG. As such, we validated that the MNNG dose-dependent death mechanism switch was not due to PARP-trapping effects.

To follow-up on the death mechanism switch, we characterized which RCD pathways MNNG was capable of inducing across doses. We found that intermediate doses of MNNG induce parthanatotic death. However, high doses of MNNG induce caspase-dependent apoptotic death. Furthermore, these two death pathways were found to be mutually exclusive. As cells experienced more apoptosis, they experienced less parthanatos. Moreover, we found that upon inhibition of parthanatos, MNNG was able to induce apoptotic death at a parthanatotic dose. And conversely, upon inhibition of apoptosis, MNNG was able to induce parthanatotic death at an apoptotic dose. This observed mutual exclusivity, between parthanatos and apoptosis, agreed with previous studies in our lab.⁴⁹

Based on the observed mutual exclusivity, we developed a model to explain the MNNG dose-dependent death mechanism switch. We predicted that DNA alkylating agent MNNG was inducing DNA damage and subsequent DNA damage response (DDR) activity. DDR activity would induce PARP-1 hyper-activation and subsequent parthanatos. Or DDR activity would induce initiation of apoptosis,

caspase activation, and subsequent apoptosis execution. In this model, the amount of DNA damage induced by MNNG, dependent on dose, influences which death pathway DDR initiates first. If apoptosis were initiated first, caspase activation would prevent subsequent parthanatos activation. This is due to the fact that apoptotic executioner Caspase-3 cleaves PARP-1, rendering it inactive and unable to initiate parthanatos.⁶⁴ However, if parthanatos were initiated first, activation of the parthanatotic pathway would inhibit subsequent apoptosis activation. This parthanatotic inhibition of apoptosis would occur through some unknown mechanism of pathway crosstalk.

To test this model, we queried whether mismatch repair (MMR), a DDR pathway, was the point at which cells decided to induce either parthanatos or apoptosis. We found that altering MMR did not alter which death pathways cells selected to execute upon MNNG treatment. This suggested that MMR was not the decision point for cell death pathway engagement. Thus, it is possible that a different DDR pathway instead serves as the decision point for death mechanism selection. Alternately, it is possible that the DDR is not involved in the decision point for death mechanism selection. Future studies will be required to further explore this phenomenon and interrogate the DDR involvement in the MNNG dose-dependent death mechanism switch.

2.2 Results

2.2A MNNG exhibits dose-dependent changes in death onset time and death rate, indicative of a death mechanism change

To explore the possibility of death polypharmacology, we focused on characterizing RCD execution after treatment with MNNG (methylnitrosoguanidine), a DNA alkylating agent. MNNG is the canonical activator of parthanatos, an inflammatory form of RCD dependent upon PARP-1 hyper-activation. We profiled MNNG response in the cervical cancer cell line HeLa, which has frequently been used to study parthanatotic death.^{53,54,56,60,83,84,85}

MNNG drug response was characterized using the FLICK assay, a fluorescent-based plate-reader assay.⁷⁵ FLICK allows for the direct measurement of dead cells across time and for the inferred calculation of total cells across time. As such, FLICK generates RV (relative viability) and FV (fractional viability) drug response data. RV is the comparison of the number of live drug-treated cells to the number of live vehicle-treated cells.⁷⁵ Alternately, FV is the comparison of the number of live drug-treated cells to the number of total (live and dead) drug-treated cells.⁷⁵ FLICK also generates LF (lethal fraction) kinetics. LF is the comparison of the number of dead drug-treated cells to the number of total (live and dead) drug-treated cells.⁷⁵

In this experiment, HeLa cells were cultured in the presence of MNNG for 48-hours. MNNG treatment induced RV defects in HeLa cells (Fig 2.1A). As MNNG

dose increased, RV defects also increased. However, MNNG displayed a more complicated dose response when analyzed through the lens of FV (Fig 2.1B). Lower doses of MNNG (up to 10uM) failed to induce cell death, despite showing RV defects. This suggested that lower doses of MNNG only induce growth arrest at this timepoint. However, intermediate doses of MNNG (greater than 10uM) induced potent cell death. The maximal amount of death was achieved at a 100uM dose of MNNG. Higher doses of MNNG (>100uM) were incapable of inducing further death at this timepoint.

This experiment was repeated with a 68-hour MNNG exposure and analyzed through the lens of LF kinetics. LF data was plotted for a single dose across time and fit to a lag-exponential model of cell death (LED).⁷⁵ The resulting plot allowed for inference of features such as death onset time and death rate. MNNG displayed unusual LF kinetics (Fig 2.1C). Lower doses of MNNG (10uM) showed no death, as expected. Intermediate doses of MNNG (31.6uM) showed a fast death onset time (> 16 hours). However, high doses of MNNG (316uM) displayed a much later death onset time (24 hours). This change in death onset time was unexpected. One would assume that higher doses result in a faster death onset time. Moreover, in spite of the delayed death onset time, the high dose of MNNG (316uM) showed a much faster death rate.

The change in death onset time and death rate suggested a change in death mechanism. To test this hypothesis, we repeated our previous FLICK experiment using HeLa treated with MNNG plus Rucaparib. Rucaparib inhibits PARP-1, thus

blocking parthanatos execution. At intermediate doses of MNNG (31.6uM), Rucaparib potently suppressed death (Fig 2.1C). This suggested that this intermediate dose was inducing parthanatotic cell death. However, at high doses of MNNG (316uM), Rucaparib exacerbated death. This suggested that the death induced by this high dose was no longer parthanatotic.

To confirm this unexpected finding, the experiment was repeated using two orthogonal assays. First, we used Cell Titer Glo, a traditional cell viability assay, to measure the drug-response of HeLa treated with MNNG, plus or minus Rucaparib, for 72-hours. This experiment was analyzed through GR (growth rate inhibition).^{77,78} GR is the comparison of drug-treated and vehicle-treated cell growth rates. Values less than one, but greater than zero, indicate partial growth arrest. Values less than zero indicate cell death. By GR, Rucaparib could only rescue intermediate doses of MNNG (Fig 2.1D). Again, this suggested that high doses of MNNG are no longer parthanatotic. Thus, this supported the hypothesis that a death mechanism switch had occurred.

Next, we used STACK, a microscopy-based assay designed to readout dead cell kinetics.⁷⁹ Like FLICK, STACK directly measures dead cells across time. However, unlike FLICK, STACK can also directly measure total cells across time.⁷⁹ To measure total cells, HeLa were labeled with a cell tracker dye prior to the start of the experiment. After labeling, HeLa cells were treated with MNNG, plus or minus Rucaparib, for 72-hours. Data was analyzed for LF. Again, this revealed that Rucaparib suppresses death induced by intermediate doses (31.6uM) of MNNG

(Fig 2.1E). However, Rucaparib exacerbates death induced by high doses (316uM) of MNNG. Again, these findings supported the death mechanism switch hypothesis.

Together, this data highlighted that cell response to MNNG was dose dependent. Low doses of MNNG induced growth arrest. Intermediate doses of MNNG induced death with a faster onset time and slower rate. This death could be blocked by Rucaparib. Therefore, intermediate doses of MNNG induce parthanatotic death. Conversely, high doses of MNNG induced death with a slower onset time and faster rate. This death was exacerbated by Rucaparib. Thus, high doses of MNNG induce non-parthanatotic death. This dose-dependent change in death onset time, death rate, and death pathway inhibitor effect, suggested that MNNG exhibits dose-dependent death mechanism changes.

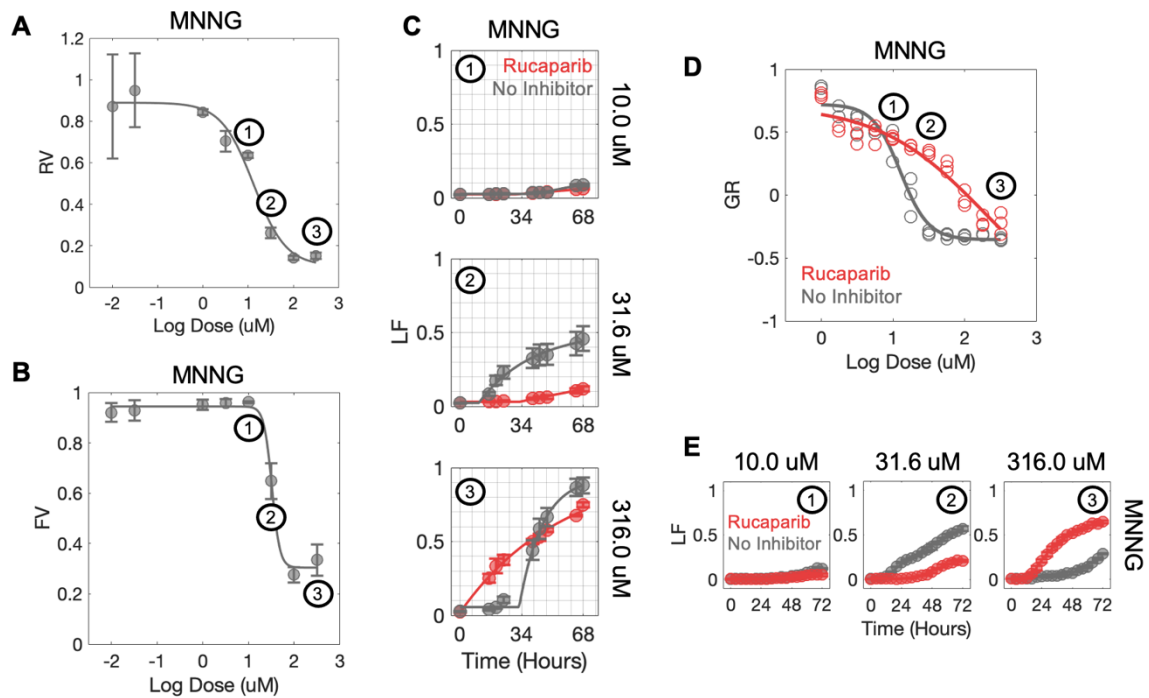


FIGURE 2.1 MNNG exhibits dose-dependent changes in death onset time and death rate, indicative of a death mechanism change. For all sub-figures, highlighted doses are 10.0uM (#1), 31.6uM (#2), and 316.0uM (#3) MNNG. **(a)** RV dose-response and **(b)** FV dose-response of HeLa cells treated with MNNG for 48 hours in the FLICK assay. **(c)** LF of HeLa cells treated with MNNG +/- Rucaparib for 68 hours in the FLICK assay. Select doses of MNNG are highlighted. **(d)** GR of HeLa cells treated with MNNG +/- Rucaparib for 72 hours via Cell Titer Glo. **(e)** LF of cell tracker-labeled HeLa cells treated with MNNG +/- Rucaparib for 72 hours in the STACK assay. Select doses of MNNG are highlighted.

2.2B MNNG dose-dependent death mechanism switch is generalizable

MNNG induces a dose-dependent death mechanism switch in HeLa cells. We sought to characterize whether this phenotype was generalizable to other cell types. A panel of cell lines of various origins (including HeLa cells) was tested via FLICK. Cells were treated with MNNG plus or minus Rucaparib for 48-hours, to look for death mechanism switches. Data was analyzed to look for FV dose-response effects. MNNG induced death in seven out of the eight cell lines tested (Fig. 2.2A). Rucaparib was able to block MNNG-induced death at specific doses in six out of the eight cell lines tested. This suggested that many cell types are capable of experiencing parthanatotic death.

Importantly, three cell lines, in addition to HeLa (cervical cancer), displayed a dose-dependent change in inhibitor effect: MCF7 (breast cancer), U2OS (osteosarcoma), and Jurkat (T cell leukemia). MCF7 and U2OS displayed the same death mechanism switch as HeLa (Fig. 2.2A). Intermediate doses of MNNG induced death that was blocked by Rucaparib. And high doses of MNNG induced death that was not blocked by Rucaparib. Thus, in MCF7 and U2OS, intermediate doses were parthanatotic and high doses were non-parthanatotic. Interestingly, Jurkat displayed an inverted death mechanism switch to HeLa (Fig. 2.2A). In Jurkat, intermediate doses of MNNG induced death that was exacerbated by Rucaparib, whereas high doses of MNNG induced death that was inhibited by Rucaparib. Thus, in Jurkat, intermediate doses were non-parthanatotic and high doses were parthanatotic.

To confirm that MCF7 and U2OS displayed the same phenotype as HeLa, the FLICK assay was repeated. MCF7 were drugged for 68-hours and U2OS were drugged for 48-hours. Data was analyzed for LF metrics. In MCF7, intermediate doses of MNNG (31.6uM) induced death with a fast onset time (<16h) that could be completely blocked by Rucaparib (Fig 2.2B). High doses of MNNG (316uM) induced death with a slower onset time (>16h) that was exacerbated by Rucaparib. U2OS showed a similar, albeit less pronounced, phenotype (Fig 2.2C). As such, these cell lines also experience parthanatotic death at intermediate doses of MNNG, but non-parthanatotic death at high doses of MNNG. Together, this data suggested that the MNNG dose-dependent death mechanism switch was a phenomenon generalizable across genetically diverse cell lines.

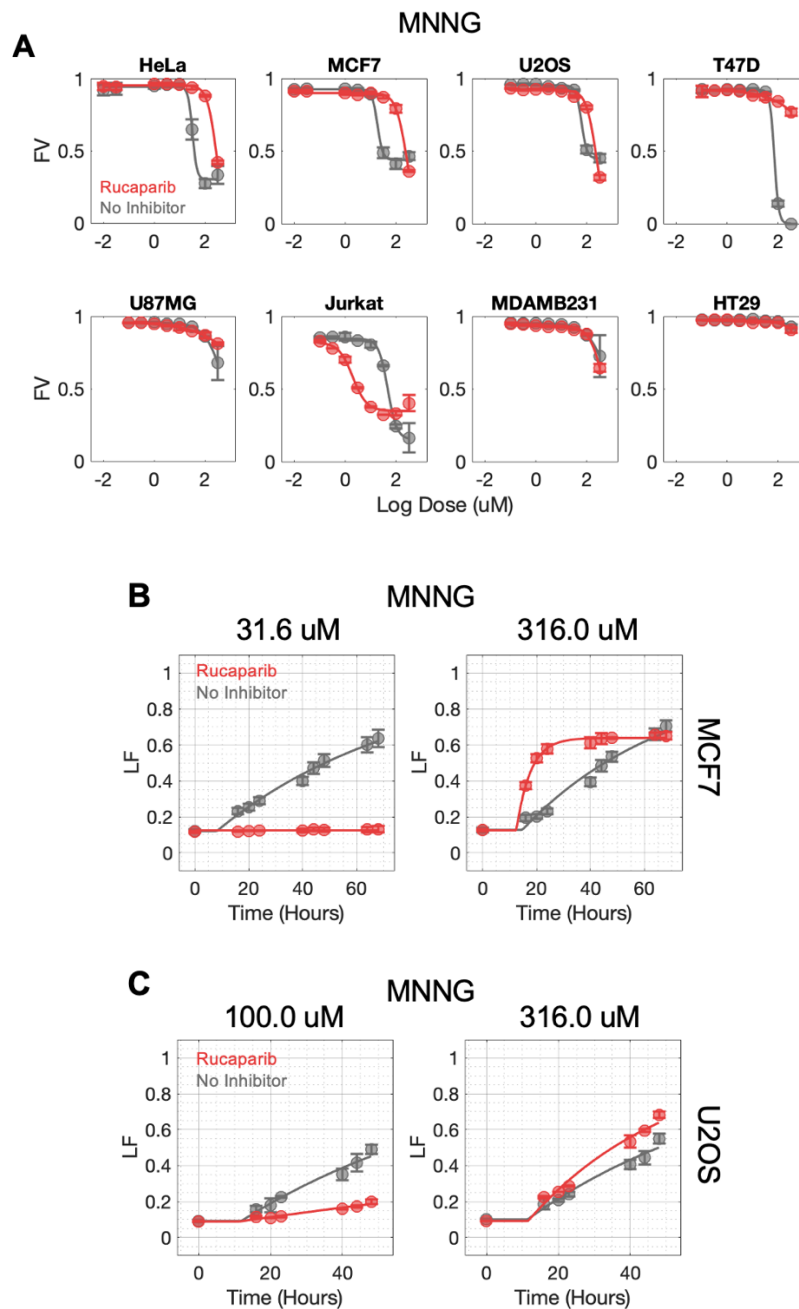


FIGURE 2.2 MNNG dose-dependent death mechanism switch is generalizable. (a) FV dose-response of cells treated with MNNG +/- Rucaparib for 48 hours in the FLICK assay. Cell type is indicated above each plot. **(b)** LF of MCF7 cells treated with MNNG +/- Rucaparib for 68 hours in the FLICK assay. Select doses of MNNG are highlighted. **(c)** LF of U2OS cells treated with MNNG +/- Rucaparib for 48 hours in the FLICK assay. Select doses of MNNG are highlighted.

2.2C MNNG dose-dependent death mechanism switch is not due to PARP-trapping effects

From our inhibitor data, we observed that Rucaparib reduced death at intermediate doses of MNNG, but exacerbated death at high doses of MNNG. This suggested that intermediate doses of MNNG induced parthanatotic death, but that high doses of MNNG induced non-parthanatotic death. However, Rucaparib inhibits PARP-1 by trapping it on DNA. PARP-trapping has been suggested to increase DNA damage, leading to increased cell death.^{81,82} As such, we were concerned that the observed phenotype was due to PARP-trapping effects rather than PARP-1-inhibition.

As such, we sought to explore whether the phenotype was an artifact of PARP-trapping. To interrogate this possibility, we utilized PARP-1 KO cells. PARP-1 KO was confirmed via western blot (Fig 2.3A). PARP-1-KO U2OS and WT-U2OS, were examined via FLICK to look at changes in MNNG FV dose-response. Cells were treated with MNNG for 48-hours. The PARP-1-KO U2OS phenocopied our previous results with Rucaparib-treated U2OS (Fig 2.3B). At intermediate doses of MNNG (31.6uM), PARP-1-KO U2OS experienced less death than WT-U2OS. However, at high doses of MNNG (316uM), PARP-1-KO U2OS experienced more death than WT-U2OS. This suggested that the previously observed results were not due to PARP-trapping exacerbating MNNG-induced death.

To confirm this finding, we repeated the FLICK assay with PARP-1-KO U2OS and WT-U2OS treated with MNNG +/- Rucaparib for 72-hours. Data was analyzed for

LF. At intermediate doses of MNNG (32uM), Rucaparib blocked death in WT-U2OS (Fig 2.3C). PARP-1-KO U2OS, plus or minus Rucaparib, showed the same level of death as WT-U2OS plus Rucaparib. Thus, PARP-1-KO phenocopied Rucaparib at intermediate MNNG doses. At high doses of MNNG (179uM), Rucaparib exacerbated death in WT-U2OS (Fig 2.3C). PARP-1-KO U2OS, plus or minus Rucaparib, showed the same level of death as WT-U2OS plus Rucaparib. Again, PARP-1-KO phenocopied Rucaparib at high MNNG doses.

This assay demonstrated that PARP-1-KO U2OS plus or minus Rucaparib phenocopied WT-U2OS plus Rucaparib. Moreover, PARP-1-KO U2OS plus Rucaparib phenocopied PARP-1-KO U2OS minus Rucaparib. Thus, we could conclude that Rucaparib was not inducing any off-target effects. As such, this data suggested that intermediate doses of MNNG are parthanatotic since death is blocked by PARP-1-inhibition (Rucaparib) or by PARP-1-KO. This data also suggested that high doses of MNNG are non-parthanatotic since death is not blocked by PARP-1-inhibition (Rucaparib) or by PARP-1-KO. Together, this data highlights that PARP-trapping does not contribute to the increased cell death observed at high doses of MNNG in the presence of Rucaparib.

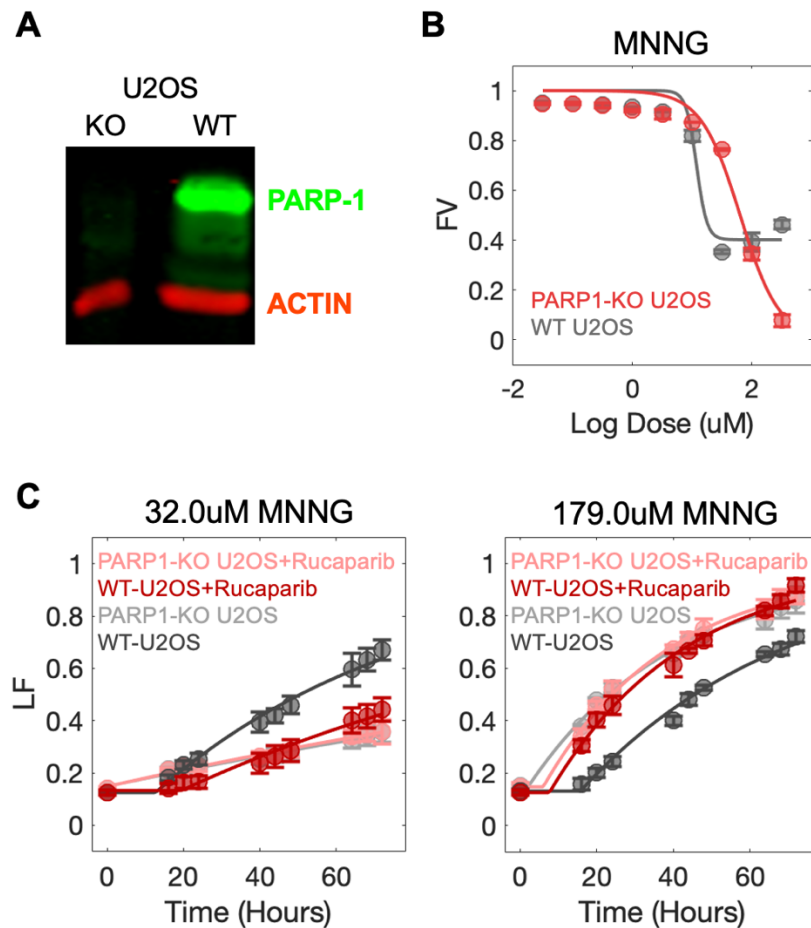


FIGURE 2.3 MNNG dose-dependent death mechanism switch is not due to PARP-trapping effects. (a) Western blot for PARP-1 protein expression in PARP-1-KO U2OS or WT-U2OS. Actin was used as a loading control. **(b)** FV dose-response of PARP-1-KO U2OS or WT-U2OS treated with MNNG for 48 hours in the FLICK assay. **(c)** LF of PARP-1-KO U2OS or WT-U2OS treated with MNNG +/- Rucaparib for 72 hours in the FLICK assay. Select doses of MNNG are highlighted.

2.2D MNNG exhibits death polypharmacology, capable of inducing either parthanatos or apoptosis

Having established the presence of an MNNG dose-dependent death mechanism switch, we sought to determine what types of death MNNG was capable of inducing. We knew that MNNG was capable of inducing parthanatotic death at intermediate doses. Death at intermediate doses was blocked by the parthanatotic inhibitor, Rucaparib, or PARP-1 knockout. However, we also knew that high doses of MNNG induced non-parthanatotic death. Death at high doses was not blocked by Rucaparib or PARP-1 knockout. It was unclear whether this non-parthanatotic death observed at high doses of MNNG was ACD (accidental cell death) or RCD (regulated cell death). Moreover, if high doses of MNNG caused RCD, it was uncertain which death pathway was being induced.

As such, we tested the HeLa response to MNNG plus or minus a panel of RCD inhibitors (Table 2.1). Cell death was read out in a 68-hour FLICK assay. The resulting data was analyzed for LF and fit to a lag exponential death (LED) model.⁷⁵ To look at the effect of RCD inhibitors across a range of killing doses, an integrated metric was developed (Fig 2.4A). The LED area under the curve (AUC) for MNNG plus inhibitor was divided by the LED AUC for MNNG alone. This resulted in a metric called Δ LED AUC. Scores greater than 1 indicated that the inhibitor had exacerbated death induced by drug. Scores less than 1 indicated that the inhibitor had protected against death induced by drug. Scores equal to 1 suggested that the inhibitor had no effect on death induced by drug.

Inhibitor	Function	Death Pathway Inhibited
Ferrostatin-1	Antioxidant	Ferroptosis
Necrostatin-1	RIPK1 Inhibitor	Necroptosis, RIPK1-Dependent Apoptosis
Rucaparib	PARP-1 Inhibitor	Parthanatos
VX-765	Caspase-1/4 Inhibitor	Pyroptosis
Z-IETD-FMK	Caspase-8 Inhibitor	Extrinsic Apoptosis
Z-VAD-FMK	Pan-Caspase Inhibitor	Apoptosis

TABLE 2.1 List of RCD pathway inhibitors. RCD inhibitors listed with their specific function and pathway.

The Δ LED AUC scores from our experiment revealed that intermediate doses of MNNG induced death that was strongly blocked by the presence of Rucaparib (Fig 2.4B). This suggested that intermediate doses were parthanatotic, matching previous expectations. However, high doses of MNNG were strongly blocked by the presence of caspase inhibitors, specifically Z-VAD-FMK. This indicated that high doses of MNNG induced apoptosis. Apoptosis is a non-inflammatory form of RCD dependent upon MOMP (mitochondrial outer membrane permeabilization) and subsequent caspase-activity.^{2,3} It is distinct from parthanatos.

To confirm these findings, we decided to use orthogonal assays to directly look at death pathway activity. Additionally, to be able to generalize these findings, we switched our experiments from HeLa to U2OS. To verify that intermediate doses of MNNG induce parthanatos, we looked for signs of parthanatotic death pathway activation. U2OS were treated with an intermediate dose of MNNG (31.6 μ M) plus or minus Rucaparib. After drug treatment, cells were harvested and assayed for expression of protein PARylation. Production of PAR indicates that PARP-1 has been hyper-activated and is a requirement for parthanatotic cell death execution.^{52,53,54} At 30 minutes post-MNNG exposure, PAR was strongly increased (Fig 2.4C). This increase in PAR was blocked by the presence of Rucaparib. Together this suggested that intermediate doses of MNNG induce parthanatotic death.

Typically, apoptotic pathway activity is monitored through expression of cleaved Caspase-3 and cleaved PARP-1. Upon initiation of apoptosis, downstream

caspses are activated via cleavage.^{2,3} Cleaved Caspase-3 subsequently induces cleavage of PARP-1.⁶⁴ However, due to only a small proportion of the population being cleaved Caspase-3/cleaved PARP-1 positive in any given moment, we could not validate direct activation of apoptosis at high doses of MNNG. Instead, to confirm that intermediate doses of MNNG induce parthanatotic death and that high doses of MNNG induce apoptotic death, we developed a co-culture assay with a flow cytometry readout.

WT-U2OS were co-cultured with either PARP-1-KO U2OS or BAK/BAX-DKO U2OS. PARP-1-KO U2OS are incapable of undergoing parthanatotic death since they do not express PARP-1. BAK/BAX-DKO U2OS are incapable of undergoing apoptotic death. BAK and BAX are required to form the pore that induces MOMP.^{2,3} Without MOMP, cells cannot undergo conventional apoptosis. In this assay, co-cultures were treated with MNNG at intermediate or high doses. One of the cell types in the co-culture was labeled with a cell tracker dye prior to the start of the assay, in order to determine of the ratio of each cell type in the co-culture. Cell tracker positive and negative cells were readout by flow cytometry at the assay endpoint, 48-hours. The ratio of cells in drug-treated co-cultures was compared to the ratio of cells in untreated co-cultures. This allowed us to test which population of cells had a survival advantage in each drug condition.

We found that PARP-1-KO U2OS had a survival advantage at intermediate doses of MNNG (Fig 2.4D). The ratio of PARP-1-KO U2OS relative to WT U2OS increased when comparing intermediate dose MNNG (50uM) co-cultures to

untreated co-cultures. Moreover, PARP-1-KO U2OS had a survival disadvantage at high doses of MNNG. The ratio of PARP-1-KO U2OS relative to WT U2OS decreased when comparing high dose MNNG (250uM) co-cultures to untreated co-cultures. We also found that BAK/BAX-DKO U2OS had a survival advantage at intermediate doses of MNNG. Importantly, the BAK/BAX-DKO U2OS had an even larger survival advantage at high doses of MNNG. The ratio of BAK/BAX-DKO U2OS relative to WT U2OS increased when comparing MNNG-treated co-cultures to untreated co-cultures. This ratio increased the most at the high dose of MNNG (250uM).

Altogether, this data suggested that intermediate doses of MNNG primarily induce parthanatotic death. Alternately, high doses of MNNG induce apoptotic death. This phenomenon was conserved across diverse cell lines and across varied assays. As such, MNNG is capable of inducing either parthanatotic or apoptotic cell death, in a dose-dependent fashion.

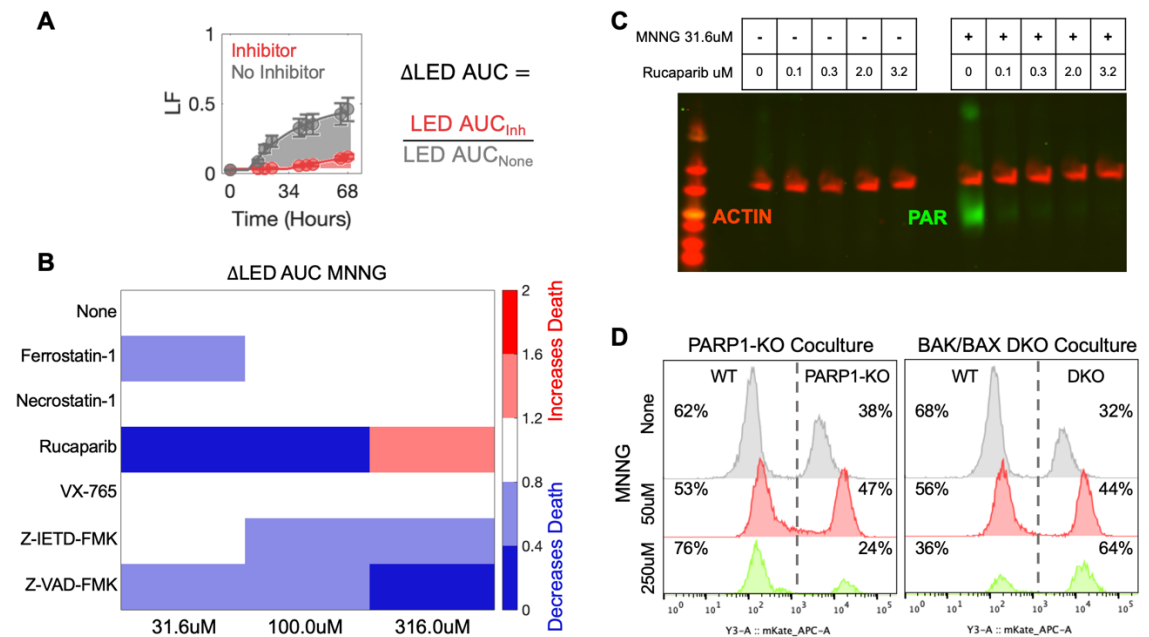


FIGURE 2.4 MNNG exhibits dose-dependent death polypharmacology, capable of parthanatos or apoptosis. (a) The $\Delta\text{LED AUC}$ metric was calculated by dividing the LED plot AUC of drug plus inhibitor by the LED plot AUC of drug alone. **(b)** $\Delta\text{LED AUC}$ of HeLa treated with MNNG +/- various cell death inhibitors for 68 hours in the FLICK assay. Select doses of MNNG are highlighted. **(c)** Western blot for PAR protein expression in U2OS exposed to 31.6uM MNNG for 30 minutes +/- Rucaparib at various doses. Actin was used as a loading control. **(d)** Co-cultures were treated with MNNG at select doses for 48 hours. WT-U2OS were unlabeled. PARP-1-KO U2OS and BAK/BAX-DKO ('DKO') U2OS were labeled with a cell tracker dye prior to the assay start. The relative proportion of each cell type in the co-culture was ascertained by flow cytometry measuring the presence of cell tracker positive and negative cells. Co-cultures were of WT-U2OS and PARP-1-KO U2OS or of WT-U2OS and BAK/BAX-DKO ('DKO') U2OS.

2.2E MNNG-induced parthanatos and apoptosis are mutually exclusive

Our finding that MNNG induces both parthanatos and apoptosis was surprising. Previous work in our lab had suggested that parthanatos and apoptosis are mutually exclusive.⁴⁹ In that study, combination of an apoptotic drug and a parthanatotic drug resulted in a reduction of the markers of activation for each pathway.⁴⁹ As such, we sought to characterize whether MNNG-induced parthanatos and apoptosis were also mutually exclusive.

To test this mutual exclusivity, we performed a quarter-log drug titration in HeLa across lethal doses of MNNG plus or minus parthanatotic inhibitor, Rucaparib, and apoptotic inhibitor, Z-VAD-FMK. Data was captured in a 68-hour FLICK assay and analyzed for LF kinetics. At 100uM of MNNG both inhibitors were roughly equally effective at blocking death (Fig 2.5A). At doses higher than 100uM, the apoptotic inhibitor was increasingly effective at blocking death. Conversely, at doses lower than 100uM, the parthanatotic inhibitor was increasingly effective at blocking death. As such, as the parthanatotic inhibitor became less effective at blocking death, the apoptotic inhibitor became more effective at blocking death. And vice versa. This suggested that the apoptotic and parthanatotic pathways might be mutually exclusive.

This FLICK data was also analyzed through the lens of Δ LED AUC scores. These scores demonstrated the degree to which the presence of inhibitor blocked death at a given drug dose. This data established that MNNG-induced death was either blocked by the apoptotic inhibitor or the parthanatotic inhibitor (Fig 2.5B). Death

induced by MNNG doses greater than 100uM was exclusively blocked by the apoptotic inhibitor when analyzed by Δ LED AUC scores. And death induced by MNNG doses less than or equal to 100uM was exclusively blocked by the parthanatotic inhibitor when analyzed by Δ LED AUC scores. As such, this also suggested that MNNG-induced apoptotic death and MNNG-induced parthanatotic death might be mutually exclusive.

To further confirm whether the apoptotic death and parthanatotic death were mutually exclusive, we tested the MNNG drug-response of WT-U2OS, PARP-1-KO U2OS, and BAK/BAX-DKO U2OS plus or minus parthanatotic and apoptotic death inhibitors. Data was captured in a 72-hour FLICK assay and analyzed for LF kinetics fit to a LED model. In WT-U2OS, death induced by high doses of MNNG (316uM) was not blocked by the parthanatotic inhibitor, Rucaparib (Fig 2.5C). However, in BAK/BAX-DKO U2OS, death induced by high doses of MNNG was completely blocked by Rucaparib (Fig 2.5C). BAK/BAX-DKO U2OS cannot undergo conventional apoptosis. This suggested that in cells where apoptosis was inhibited, high doses of MNNG could switch back to a parthanatotic form of cell death.

Likewise, in WT-U2OS, the apoptotic inhibitor, Z-VAD-FMK, failed to protect against death induced by intermediate doses of MNNG (32uM) (Fig 2.5D). However, in PARP-1-KO U2OS, Z-VAD-FMK was able to rescue death induced by intermediate doses of MNNG (Fig 2.5D). PARP-1-KO U2OS cannot undergo parthanatos. This suggested that in cells where parthanatos was inhibited,

intermediate doses of MNNG could switch back to inducing an apoptotic form of cell death.

Together, this data provided evidence that MNNG-induced apoptosis and parthanatos are mutually exclusive. As such we built a model that fit our expectations based on the available data (Fig 2.5E). MNNG is a DNA alkylating agent that induces DNA damage.⁸⁶ Upon DNA damage, the DNA damage response (DDR) is activated.^{87,88,89} In this model, the amount of DNA damage induced by MNNG, dependent on dose, influences which death pathway the DDR initiates first. Activation of the DDR can lead to hyper-activation of PARP-1 and subsequent execution of parthanatotic death.⁵⁴ Or activation of the DDR can lead to initiation of the apoptotic death pathway, downstream caspase activation, and subsequent execution of apoptotic death.⁸⁷

As such, the first death pathway turned on by DDR activity suppresses the other death pathway. Active caspases, specifically Caspase-3, cleave PARP-1, inhibiting PARP-1 function.⁶⁴ Thus, activation of apoptosis is already known to cause inhibition of parthanatos. However, it is unclear how activation of parthanatos is able to inhibit apoptosis. Our current understanding of these two death pathways does not provide a mechanism for such inhibitory pathway crosstalk. Moreover, our model assumes that altered DDR activity, driven by MNNG dose, is responsible for the cell's decision to undergo either apoptosis or parthanatos. Yet, it is unclear whether the DDR actually serves as the death pathway decision point upon MNNG treatment. Although this proposed model has

several unknowns, it is able to explain why parthanatos and apoptosis are mutually exclusive when induced by MNNG.

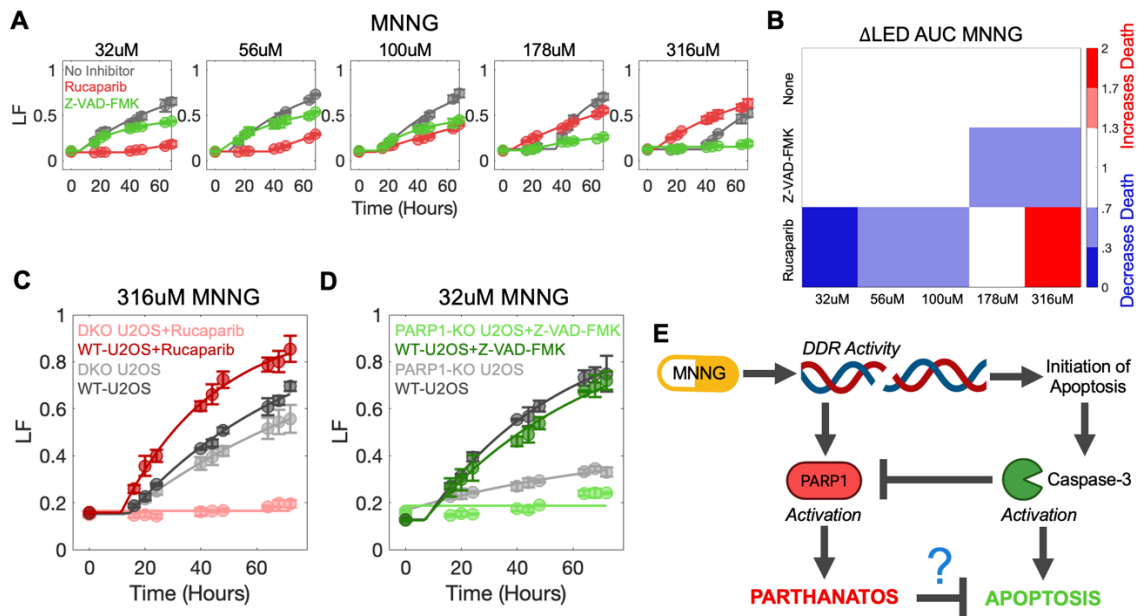


FIGURE 2.5 MNNG-induced parthanatos and apoptosis are mutually exclusive. (a) LF of HeLa treated with MNNG +/- Rucaparib or Z-VAD-FMK for 68 hours in the FLICK assay. Select doses of MNNG are highlighted. **(b)** Δ LED AUC of HeLa treated with MNNG +/- Rucaparib or Z-VAD-FMK for 68 hours in the FLICK assay. Select doses of MNNG are highlighted. **(c)** LF of WT-U2OS or BAK/BAX-DKO ('DKO') U2OS treated with MNNG +/- Rucaparib for 72 hours in the FLICK assay. Select doses of MNNG are highlighted. **(d)** LF of WT-U2OS or PARP-1-KO U2OS treated with MNNG +/- Z-VAD-FMK for 72 hours in the FLICK assay. Select doses of MNNG are highlighted. **(e)** Model of mutual exclusivity between parthanatos and apoptosis. MNNG induces DNA damage, which activates the DDR. DDR activity can induce PARP-1 hyper-activation and downstream parthanatos execution. DDR activity can also induce initiation of apoptosis, downstream caspase activation, and execution of apoptosis. Apoptosis can inhibit parthanatos through Caspase-3 cleavage of PARP-1. It is unclear how parthanatos inhibits apoptosis. This model predicts that the cell decision point for death pathway activation occurs at the DDR. MNNG dose drives different levels of DNA damage which alter DDR activity. This altered DDR activity changes which death pathway the DDR initiates first. *Created with BioRender.com.*

2.2F MNNG death polypharmacology is not due to altered MMR response

To attempt to validate our model, we decided to test whether altered DDR activity resulted in a switch in MNNG death mechanism. We started by interrogating whether altering MMR (mismatch repair), a DDR pathway, could alter MNNG death pathway selection. The MMR is engaged when cells undergo replication errors.^{87,90,91} Importantly, it has been documented that DNA alkylation, specifically MNNG, induces activation of the MMR pathway in HeLa cells.⁹² In this study, Peng *et al* found that MMR-proficient HeLa undergo Chk1 activation and subsequent growth arrest after MNNG-treatment.⁹² Conversely, MMR-deficient HeLa show no Chk1 activation after MNNG-treatment.⁹² Chk1 serves as a general marker of DDR activation.⁸⁷

The MMR pathway involves the use of several proteins, one of which being MSH2. MSH2 serves as the mismatch recognition factor.⁹¹ Thus, MSH2 knockout renders cells unable to use the MMR pathway. Several cell lines have been generated with MSH2-KO (Fig 2.6A). HeLa cells are naturally MMR proficient. Knockout of MSH2 renders them MMR-deficient.^{91,92} Conversely, Hec59 cells are naturally MMR deficient due to loss of chromosome 2. Re-introduction of chromosome 2 restores Hec59 ability to undergo MMR.⁹¹ These MMR proficient and MMR deficient HeLa and Hec59 cell lines were generous gifts from the S. Cantor Lab (UMass Chan Medical School).

We tested how MMR-deficiency altered cell response to MNNG. Specifically, we profiled WT-HeLa (MMR-proficient), MSH2-KO HeLa (MMR-deficient), WT-Hec59

(MMR-deficient), and Chr2+ Hec59 (MMR proficient) in a FLICK assay. Cells were treated with MNNG for 72 hours plus or minus apoptotic (Z-VAD-FMK) and parthanatotic (Rucaparib) inhibitors. FLICK data was analyzed to obtain RV and FV metrics. We expected that if MMR was the decision point for the cell to induce either parthanatos or apoptosis, that removing MMR would alter which death pathway the cell would induce. Specifically, we expected that the degree to which a given death inhibitor would block death at a given dose would change in the MMR-proficient and MMR-deficient backgrounds.

We found that MMR-proficient HeLa were more sensitive than MMR-deficient HeLa to MNNG by RV (Fig 2.6B). This agreed with previous studies.⁹² Interestingly, MMR-deficient HeLa showed increased RV defects in the presence of Rucaparib. No clear phenotypes were observable when comparing RV metrics of MMR-deficient and MMR-proficient Hec59. The lack of observable RV phenotypes when comparing the Hec59 cells could be due to the shorter assay time-course of 72 hours. This assay timepoint was optimized to capture FV effects at high doses of MNNG. It was not designed to capture long-term RV defects.

Additionally, no clear FV changes were observable when comparing FV metrics of MMR-deficient and MMR-proficient cells (Fig 2.6C). Importantly, the lack of FV phenotype suggested that the MMR was not the point at which cells would decide to undergo either apoptosis or parthanatos upon MNNG treatment. Thus, it is possible that a different DDR pathway serves as the decision point for death pathway selection after MNNG treatment. If an alternate DDR pathway serves as

the cell decision point, our current model of MNNG death polypharmacology remains correct. However, it is also possible that the DDR is not involved in the decision point for death pathway selection after MNNG treatment. If the DDR is not the cell decision point, our current model of MNNG death polypharmacology is incorrect.

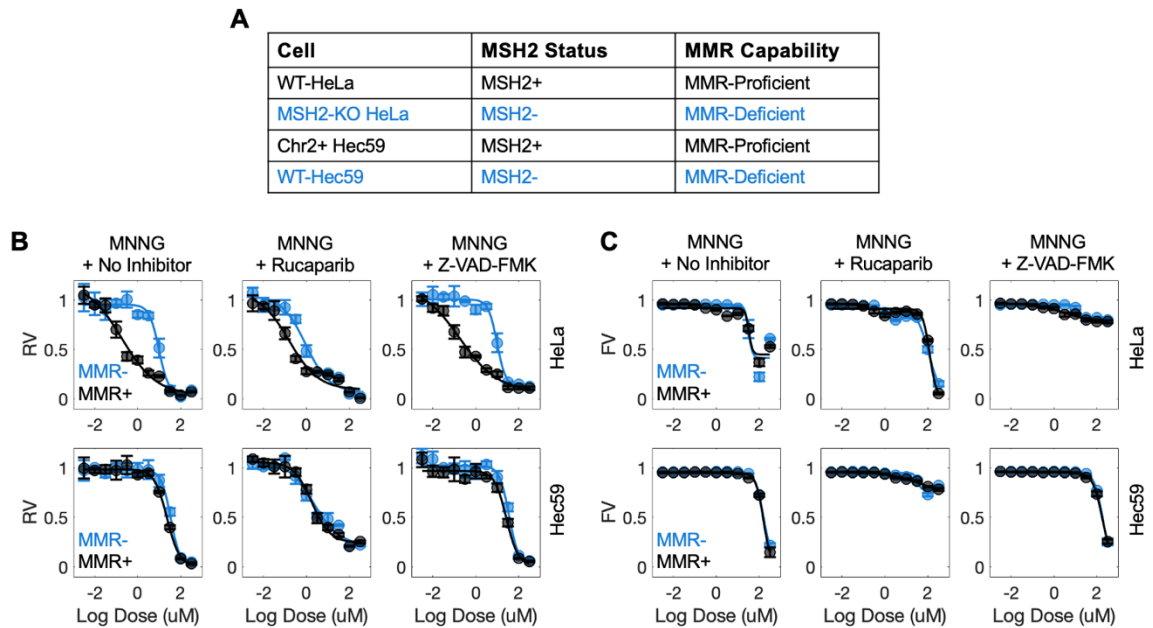


FIGURE 2.6 MNNG death polypharmacology is not due to altered MMR response. (a) Schematic of MMR proficient and deficient cell lines used in subsequent assays. These cell lines were generous gifts from the S. Cantor Lab (UMass Chan Medical School). (b) RV dose-response of MMR-proficient and MMR-deficient HeLa or Hec59 cells treated with MNNG +/- Rucaparib or Z-VAD-FMK for 72 hours in the FLICK assay. (c) FV dose-response of MMR-proficient and MMR-deficient HeLa or Hec59 cells treated with MNNG +/- Rucaparib or Z-VAD-FMK for 72 hours in the FLICK assay.

2.3 Discussion

In this study, we focused on characterizing MNNG, a DNA alkylating agent known to induce parthanatos. We found that MNNG displays a dose-dependent death mechanism switch. MNNG induces unusual death kinetics across doses. Low doses of MNNG induce no death; intermediate doses of MNNG induce death with a faster onset time but slower rate; and high doses of MNNG induce death with a slower onset time but faster rate. Importantly, Rucaparib, which inhibits parthanatos, only blocks death at intermediate doses of MNNG. Instead, Rucaparib exacerbates death induced by high doses of MNNG. Thus, intermediate MNNG doses are parthanatotic and high MNNG doses are non-parthanatotic. Together, this data suggested that MNNG had induced a dose-dependent death mechanism switch.

Moreover, in this study we found that the MNNG dose-dependent death mechanism switch was observable across genetically diverse cell types. This suggested that the death mechanism switch was generalizable. Additionally, we found that this phenomenon was not due to an artifact caused by PARP-trapping. PARP-1-KO cells displayed the same phenotype as Rucaparib-treated PARP-1-expressing cells. Together, this data suggested that the observed dose-dependent death mechanism switch was a real and generalizable phenomenon.

To fully establish this phenotype, we sought to characterize what RCD pathways MNNG was able to execute. We found that MNNG was capable of inducing both parthanatos and apoptosis. Intermediate doses of MNNG induce parthanatos; high doses of MNNG induce apoptosis. Moreover, these two death pathways were found to be mutually exclusive. As cells experienced more apoptosis, they experienced less parthanatos. And vice versa. Additionally, upon inhibition of parthanatos, MNNG was able to induce apoptosis. And, upon inhibition of apoptosis, MNNG was able to induce parthanatos. This observed mutual exclusivity between the parthanatos death pathway and apoptosis death pathway agreed with previous studies from our lab.⁴⁹

As such, we developed a model to explain the MNNG dose-dependent death mechanism switch. This model was based on the observed mutual exclusivity between apoptosis and parthanatos. In this model, MNNG induces DNA damage and subsequent DDR activity. DDR activity can initiate either apoptosis or parthanatos. Apoptosis is capable of inhibiting parthanatos through Caspase-3 cleavage of PARP-1.⁶⁴ Parthanatos is capable of inhibiting apoptosis through some unknown mechanism. As such, the first pathway turned on by DDR activity suppresses the other pathway. In this model, MNNG dose determines the level of DNA damage. The level of DNA damage determines DDR activity. And DDR activity alters which death pathway is activated first. Therefore, this model assumes that the DDR is the point at which cells decide to induce either parthanatos or apoptosis.

To test this model, we queried whether mismatch repair (MMR), a DDR pathway, was the point at which cells decided to induce either parthanatos or apoptosis. We focused on MMR since it has been documented that DNA alkylation, specifically MNNG, induces activation of the MMR pathway in HeLa cells.⁹² We found that altering MMR did not alter which death pathways cells selected to execute. This suggested that MMR was not the point at which cells would decide to undergo either apoptosis or parthanatos upon MNNG treatment. Thus, a different DDR pathway might serve as the decision point for death mechanism. If a different DDR pathway is the decision point, then our current model of MNNG dose-dependent death polypharmacology remains correct. Alternately, it is possible that the DDR is not involved in the decision point of death mechanism. If the DDR is not the decision point, then our current model of MNNG dose-dependent death polypharmacology is incorrect.

Our study reveals the existence of dose-dependent death polypharmacology. We found that MNNG is capable of altering which death pathway is executed depending on the administered dose. The existence of dose-dependent death polypharmacology has important considerations for clinical therapies. Foremost, it highlights the importance dose selection for patients. Using MNNG as a hypothetical example, apoptotic high doses of MNNG would potentially be less effective in an apoptotic-resistant tumor type. In this situation, the patient would instead benefit from parthanatotic intermediate doses of MNNG.

Second, this study highlights the importance of death pathway interactions and death polypharmacology in rational combination design. Most clinical cancer treatments rely on combination drug therapies.⁶⁶ Combination therapy outcomes can be determined by death pathway interactions. We expect that antagonistic death pathway interactions will result in less cell death. For chemotherapies, less cell death could result in worse clinical outcomes. Our predictions of death pathway interactions are complicated by the existence of death polypharmacology. As such, we might find that dose-selection would alter expected drug combination outcomes. For example, drug combination outcomes of MNNG plus an apoptotic agent would likely be determined by MNNG dose. Apoptosis and parthanatos are mutually exclusive. Intermediate doses of MNNG induce parthanatos. High doses of MNNG induce apoptosis. Thus, intermediate MNNG dose plus apoptotic agent would result in less death. However high MNNG dose plus apoptotic agent would result in more death. Thus, this highlights how death polypharmacology can play a critical role in drug combination outcomes.

While MNNG serves as a good tool compound for studying parthanatotic death, MNNG is not a clinically relevant agent. However, clinically relevant agents exist that have been noted to induce death polypharmacology. The clinical agent Sorafenib has been reported to induce ferroptosis in some cancer contexts and apoptosis in other cancer contexts.^{2,68,69,70,71,72} Moreover, the clinical agent Doxorubicin is known to induce apoptosis in some cancer contexts and necroptosis

in other cancer contexts.^{73,74} This shows that death polypharmacology is a real and clinically relevant phenomenon.

As such, this study highlights that death pathway execution can change across dose or across different genetic contexts. This death polypharmacology has important clinical ramifications. Foremost, due to frequent cancer cell evasion of apoptosis,¹ there will likely be a push to develop more non-apoptotic therapeutics. As more non-apoptotic agents are designed and introduced into the clinic, it will be necessary to carefully characterize RCD pathway engagement. Since death polypharmacology can alter death pathway selection, RCD pathway engagement must be monitored across dose and genetic context. Moreover, as these non-apoptotic agents are introduced into combination therapies, it will be necessary to improve our current understanding of RCD pathway interactions. Characterization of drug death pathway engagement and RCD interactions will allow us to improve rational drug combination design.

2.4 Materials and Methods

2.4A Cell lines

All cell lines were maintained at low passage, no more than 20 passages from the original vial. Cells were cultured in an incubator (37°C, 5% CO₂). HeLa, MDA-MB-

231, MCF7, U2OS, and U87-MG were maintained in Dulbecco's Modified Eagle Medium (DMEM) (Corning, Cat# 10-017-CV or Thermo, Cat# 11965118) supplemented with 10% fetal bovine serum (FBS) (Peak Serum, Cat#PS-FB2, Lot#21E1202 or ThermoFisher Scientific, Cat# SH30910.03, Lot# SH40014-13), 2mM glutamine (ThermoFisher Scientific, Cat# MT25005CI), and 1% penicillin-streptomycin (ThermoFisher Scientific, Cat# MT30002CI). T47D and Jurkat were maintained in Roswell Park Memorial Institute-1640 (RPMI-1640) (Gibco, Cat# 11875119) supplemented with 10% FBS, 2mM glutamine, and 1% penicillin-streptomycin. HT29 were maintained in McCoy's 5A Medium (Fisher Scientific, Cat#10-050-CV) supplemented with 10% FBS and 1% penicillin-streptomycin.

For the MMR studies, WT-HeLa, MSH2-KO HeLa, Chr2+ Hec59, and WT-Hec59 were generous gifts from the S. Cantor Lab (UMass Chan Medical School). WT-HeLa and MSH2-KO HeLa were maintained in DMEM supplemented with 10% FBS, 2mM glutamine, and 1% penicillin-streptomycin. Chr2+ Hec59 and WT-Hec59 were maintained in DMEM supplemented with 15% FBS, 2mM glutamine, and 1% penicillin-streptomycin.

All cell lines were cultured in 10cm dishes (Fisherbrand Scientific, Cat# FB012924) or 15cm dishes (USA Scientific, Cat# CC7682-3614).

2.4B General reagents

MNNG was purchased from Biosynth Carbosynth (Cat# FM11256) or VWR (Cat# TCM0527-005G). Rucaparib (Cat# S1098), Necrostatin-1 (Cat# S8037), and Ferrostatin-1 (Cat# S7243) were purchased from SelleckChem. Z-VAD-FMK (Cat# A1902), Z-IETD-FMK (Cat# B3232), and VX-765 (Cat# A8238) were obtained from ApexBio. Sytox Green Nucleic Acid Stain (Cat# S7020) and Cell Tracker Deep Red (Cat# C34565) were purchased from ThermoFisher Scientific (Cat# S7020). Cell Titer Glo was purchased from Promega (Cat# G7571). Puromycin was purchased from Corning (Cat# 62111-170). Anti poly/mono ADP ribose rabbit monoclonal antibody (Cat# 83732) and anti PARP-1 rabbit monoclonal antibody (Cat# 9532S) were purchased from Cell Signaling Technologies. Anti β -actin monoclonal mouse antibody (Cat# A2228-200uL) was purchased from Sigma Aldrich. Secondary antibodies goat anti-mouse IRDye 680RD (Cat# 926-68070) and goat anti-rabbit IRDye 800CW (Cat# 926-32211) were purchased from Li-Cor. The cOmplete protease inhibitor cocktail (Cat# 11697498001) and the PhosSTOP phosphatase inhibitor tablets (Cat# 4906845001) were purchased from Millipore Sigma.

2.4C BAK/BAX-DKO U2OS and PARP-1-KO U2OS cell line generation

BAK/BAX-DKO U2OS were generated as described in Richards *et al* (2020).⁴⁹ PARP-1-KO U2OS were generated using the PX330-puro plasmid with an hSpCas9 and *PARP-1* (CGAGTCGAGTACGCCAAGAG) sgRNA insert. U2OS

cells were transiently transfected using FuGENE HD transfection reagent (Promega, Cat# E2311). Cells were selected with 10ug/mL puromycin. Following puromycin selection, cells were seeded as single-cell clones. PARP-1-KO was confirmed by western blot and sequencing.

2.4D FLICK assay

FLICK was carried out according to the protocol described in Richards *et al* (2021).⁷⁵ Cells were trypsinized and counted using a hemocytometer. Cells were plated in 96-well optical-bottom, black-walled plates (Corning, Cat# 3904 or VWR, Cat# 655090). Cells were seeded in 80uL of media per well at 1000-5000 cells per well, depending on the assay length and cell line growth rate. Plates were returned to the incubator (37°C, 5% CO₂) to attach to the well before addition of inhibitor or drug. Inhibitor was diluted to a 10X stock in media containing 50uM sytox green. Inhibitor dilutions were prepared in 96-well U-bottom storage plates (Corning, Cat# 07-200-95). 10uL of 10X inhibitor in 50uM sytox green was added to each well. Drug was also diluted to a 10X stock in media. Drug dilutions were prepared in 96-well U-bottom storage plates. 10uL of 10X drug was added to each well. The final well volume was at 100uL, with 1X inhibitor, 1X drug, and 5uM sytox green. Plates were returned to the incubator (37°C, 5% CO₂). If the experiment was completed without inhibitor, the inhibitor dilution was omitted. In this case, sytox was added at the drug dilution step.

Fluorescence readings were taken at the indicated timepoints using a Tecan Spark microplate reader (Serial# 1711001194). Fluorescence was set to an excitation/emission of 503/524. Fluorescence gain was set for each cell line to achieve linearity below the saturation limit of the detector. Plates were returned to the incubator (37°C, 5% CO₂) in between fluorescence readings. At the start of each experiment, one plate was permeabilized to obtain starting total fluorescence. At the end of each experiment, each remaining plate was permeabilized to obtain ending total fluorescence. Cells were permeabilized using 10uL of 1% TritonX-100 (Fisher, Cat# BP151-500) and incubated at 37C for >2 hours. FLICK data was analyzed as described in section 2.4I Data analysis.

2.4E Cell Titer Glo assay

Cells were trypsinized and counted using a hemocytometer. Cells were plated in 96-well optical-bottom, black-walled plates (VWR, Cat# 655090). Cells were seeded in 80uL of media per well at 1000-5000 cells per well, depending on the assay length and cell line growth rate. Cells were returned to the incubator (37°C, 5% CO₂) to attach to the well before addition of inhibitor or drug. Inhibitor was diluted to a 10X stock in media. Inhibitor dilutions were prepared in 96-well U-bottom storage plates (Corning, Cat# 07-200-95). 10uL of 10X inhibitor was added to each well. Drug was also diluted to a 10X stock in media. Drug dilutions were prepared in 96-well U-bottom storage plates. 10uL of 10X drug was added to each well. The final well volume was at 100uL, with 1X inhibitor and 1X drug.

Plates were returned to the incubator (37°C, 5% CO₂) until assay endpoint. At the start of each experiment, one plate was analyzed by Cell Titer Glo to determine starting cell luminescence. At the end of each experiment, the remaining plates were analyzed by Cell Titer Glo to determine ending cell luminescence. Plates were moved to RT for at least 30 minutes prior to addition of Cell Titer Glo reagents. Cell Titer Glo (Promega, Cat# G7571) reagents were brought to RT completely before the addition to plates. 33uL of Cell Titer Glo reagent was added to each well. Plates were then agitated for 2 minutes. After a 10-minute incubation, 100uL of each well was transferred to a well in a white, opaque 96-well plate for luminescence detection on a Tecan Spark microplate reader (Serial# 1711001194). Cell Titer Glo data was analyzed as described in section 2.4I Data analysis.

2.4F STACK assay

STACK was carried out according to the protocol described in Forcina *et al.*⁷⁹ Cells were trypsinized and counted using a hemocytometer. Prior to plating, cells were stained with Cell Tracker Deep Red according to manufacturer instructions. Cells were plated in 96-well optical-bottom, black-walled plates (Corning, Cat# 3904). Cells were seeded in 80uL of media per well at 1000-5000 cells per well, depending on the assay length and cell line growth rate. Cells were returned to the incubator (37°C, 5% CO₂) to attach to the well before addition of inhibitor or drug. Inhibitor was diluted to a 10X stock in media containing 500nM sytox green.

Inhibitor dilutions were prepared in 96-well U-bottom storage plates (Corning, Cat# 07-200-95). 10uL of 10X inhibitor in 500nM sytox green was added to each well. Drug was also diluted to a 10X stock in media. Drug dilutions were prepared in 96-well U-bottom storage plates. 10uL of 10X drug was added to each well. The final well volume was at 100uL, with 1X inhibitor, 1X drug, and 50nM sytox green.

After drug addition, plates were transferred to an IncuCyte S3 automated microscope (Essen Biosciences) with a built-in incubator (37°C, 5% CO₂). Images were collected using the following settings: green channel (excitation 460±20, emission 524±20, acquisition time 300ms) and red channel (excitation 585±20, emission 635±70, acquisition time 400ms). Plates were imaged every 4 hours for the duration of the assay. STACK data was analyzed as described in section 2.4I Data analysis.

2.4G Western blot assay

To generate PARP-1-KO U2OS lysates and WT-U2OS lysates, cells were seeded in 10cm dishes and placed in an incubator (37°C, 5% CO₂). Once cells had reached near confluency, media was aspirated. Dishes were then washed twice with 2mL of cold PBS. Cells were then lysed using 500uL of sodium dodecyl sulfate (SDS)- lysis buffer (50mM Tris-HCl, 2% SDS, 5% glycerol, 5mM EDTA, 1mM NAF, 10mM β-GP, 1mM PMSF, 1mM Na₃VO₄, protease inhibitor, and phosphatase inhibitor). After addition of lysis buffer, dishes were stored at -20C.

To generate the U2OS lysates for monitoring PAR, WT-U2OS were seeded at 250,000 cells per well in 6-well plates (USA Scientific, Cat# 5665-7160Q). Plates were then returned to an incubator (37°C, 5% CO₂). The day following plating, cells were primed with Rucaparib at the specified concentrations. Again, plates were then returned to an incubator (37°C, 5% CO₂). The day following priming, cells were treated with 31.6uM MNNG. Cells were harvested at the specified timepoints. Media was aspirated. Plates were then washed twice with 2mL of cold PBS. Cells were then lysed using 150uL of SDS-lysis buffer. After addition of lysis buffer, plates were stored at -20C.

Lysates were allowed to thaw to RT and harvested using cell scrapers. Lysates were then transferred to 0.2uM multi-well filters (Pall, Cat# 5053) and centrifuged to remove DNA contamination. Lysate protein concentration was then determined using the Pierce BCA Protein Assay Kit (ThermoFisher Scientific, Cat# 23225). Lysates were normalized to the lowest sample for SDS-PAGE loading. Lysates were loaded onto pre-cast 8% 48-Well E-PAGE gels (ThermoFisher Scientific, Cat# EP04808) and transferred using the iBlot system (ThermoFisher Scientific) onto nitrocellulose membranes (ThermoFisher Scientific, Cat# IB301001).

Blots were blocked with 1:1 Odyssey Blocking Buffer (Li-Cor, Cat# 27-40000) in phosphate buffered saline (PBS) for 1 hours at RT. Primary antibodies were diluted into 1:1 Odyssey Blocking Buffer in phosphate buffered saline with 0.1% Tween (PBST) and incubated overnight at 4C. Anti poly/mono ADP ribose rabbit monoclonal antibody (Cell Signaling Technologies, Cat# 83732) was diluted

1:1000. Anti PARP-1 rabbit monoclonal antibody (Cell Signaling Technologies, Cat# 9532S) was diluted 1:1000. After overnight primary antibody incubation, blots were moved to RT for 1 hour. Anti β -actin monoclonal mouse antibody (Sigma Aldrich, Cat# A2228-200uL) was spiked in at a 1:15000 dilution. Blots were incubated at RT for another 1 hour. Blots were then washed two times in PBST for 5 minutes. Secondary antibodies were diluted into 1:1 Odyssey Blocking Buffer in PBST and incubated for 1 hour at RT. Secondary antibodies goat anti-mouse IRDye 680RD (Li-Cor, Cat# 926-68070) and goat anti-rabbit IRDye 800CW (Li-Cor, Cat# 926-32211) were each diluted 1:15000. After incubation, blots were then washed four times in PBST for 5 minutes. Blots were then washed in PBS.

After staining was complete, blots were imaged using the Li-Cor Odyssey CLx Scanner. Images were analyzed using the Li-Cor Image Studio Software.

2.4H Flow cytometry co-culture assay

Cells were trypsinized and counted using a hemocytometer. Prior to plating, BAK/BAX-DKO U2OS and PAR1-KO U2OS cells were stained with Cell Tracker Deep Red. WT-U2OS were left unstained. Cells were seeded at 100,000-800,000 cells per well in 6-well plates, depending on expected growth and death rates upon drug treatment. Some wells were seeded as mono-culture controls. Other wells were seeded as co-culture controls, with co-cultures of BAK/BAX-DKO U2OS and WT-U2OS or with co-cultures of PARP-1-KO U2OS and WT-U2OS. Plates were

returned to the incubator (37°C, 5% CO₂) overnight before addition of drug. Cells were then treated with MNNG at 50uM or 250uM. Plates were then returned to the incubator (37°C, 5% CO₂) until assay completion.

After 48 hours of drug treatment, cells were trypsinized and harvested. Flow cytometry data, monitoring changes in Cell Tracker Deep Red positive and negative cells, was collected using the MACSQuant VYB (Serial# 3143). Flow cytometry co-culture data was then analyzed as described in section 2.4I Data Analysis.

2.4I Data analysis

FLICK data was analyzed in MATLAB, as described in Richards *et al* (2021),⁷⁵ to produce RV dose-response data, FV dose-response data, kinetic LF data, LED kinetics, death onset metrics, and death rate metrics. Cell Titer Glo data was analyzed in MATLAB, as described in Hafner *et al* (2016),^{77,78} to produce GR dose-response data. STACK data was analyzed in MATLAB, as described in Richards *et al* (2021), Schwartz *et al*, and Forcina *et al*,^{75,76,79} to produce kinetic LF data and LED kinetics.

Flow cytometry data was analyzed using FlowJo (v 10.5.3). Live cells were first gated on using FSC/SSC. The fraction of Cell Tracker Deep Red positive and negative cells was determined using a histogram of APC⁺ live cells and APC⁻ live cells.

CHAPTER III: DISCUSSION

3.1 Death Polypharmacology Considerations for Cancer Therapies

Our study uncovers the phenomenon of death polypharmacology. Death polypharmacology occurs when a drug engages multiple RCD pathways. In particular, we found evidence of a dose-dependent death polypharmacology. Dose-dependent death polypharmacology occurs when the death pathway selection is tunable by drug dose. This means that one dose induces one death pathway, whereas another dose induces a different death pathway. Specifically, we found that MNNG, a DNA alkylating agent, is capable of altering which death pathway is executed in a dose-dependent fashion. MNNG can induce two distinct RCD pathways. Intermediate doses induce parthanatos, an inflammatory PARP-1-dependent death. And high doses induce apoptosis, a non-inflammatory caspase-dependent death. Such dose-dependent death polypharmacology is important to consider for clinical therapy outcomes. Since it is a tunable phenomenon, such that altering the dose changes which death pathway is engaged, it can be controlled. As such, this study highlights the importance of dose selection for optimization of clinical cancer therapies.

Dose selection had long been considered an important factor in clinical treatment outcome. Studies of alkylating agents *in vivo* noted that drug dose and tumor reduction were proportional, until a maximum effect was achieved.^{93,94,95,96} As such, trials were initiated to test the effect of intermediate dose chemotherapy versus high dose chemotherapy in humans.^{93,97,98,99} However, in these trials, high doses showed no benefit in survival over intermediate doses. This failure highlighted that experimental results cannot be translated directly into clinical outcomes.⁹³ Homogeneous cell lines cannot capture the complexity of tumors.^{93,100} As such, these studies emphasize that dose selection is still a challenge within the cancer field.

The existence of death polypharmacology further complicates dose selection. We have shown that MNNG is capable of inducing multiple forms of death *in vitro*, in a dose-dependent fashion. It is likely that other drugs also demonstrate this phenomenon. The specific RCD pathway induced by a drug could enhance or confound treatment outcomes. For instance, many cancers have developed means of evading apoptotic death.^{1,21,22} Therefore, selecting drug doses that induce non-apoptotic RCD could improve clinical outcomes in some instances. Additionally, as immunotherapies become more prevalent, it might be beneficial to pair immunotherapies with drugs that induce inflammatory forms of cell death, such as ferroptosis, necroptosis, or parthanatos. Again, selecting doses that induce non-apoptotic RCD could improve clinical outcomes in this situation. As such, it is

necessary to understand whether the phenomenon of dose-dependent death polypharmacology translates to *in vivo* studies and to clinical patients.

There is already evidence that death polypharmacology exists in the clinic. The clinical agent Sorafenib has been reported to induce ferroptosis in some cancer contexts and apoptosis in other cancer contexts.^{2,68,69,70,71,72} Moreover, the clinical agent Doxorubicin is known to induce apoptosis in some cancer contexts and necroptosis in other cancer contexts.^{73,74} As such, these studies highlight that death polypharmacology is a real and observable phenomenon. However, it is challenging to discern whether the observed death polypharmacology is genetic context dependent, dose dependent, or non-specific. For this reason, it is important to further explore and characterize instances of death polypharmacology, especially in clinical agents.

This study also underscores the importance of death polypharmacology and RCD pathway interactions. Most clinical cancer treatments rely on combination drug therapies.⁶⁶ Combination therapy could utilize two drugs that induce different forms of death. This would force a death pathway interaction. Other work from our lab has shown that RCD interactions are largely antagonistic; activation of one death pathway inhibits the activation of another death pathway.⁴⁹ As such, combining two drugs that activate different death pathways could result in less cell death than expected. Such an outcome would hamper clinical therapeutic efficacy. For this reason, RCD pathway interactions need to be characterized.

Our study establishes a specific RCD pathway interaction with potential clinical utility. We found that apoptosis and parthanatos are mutually exclusive. Activation of apoptosis inhibits execution of parthanatos. Conversely, activation of parthanatos inhibits execution of apoptosis. This phenomenon was also reported by our lab in Richards *et al* (2020).⁴⁹ This study demonstrated that drug combination of parthanatotic agents and apoptotic agents resulted in less cell death than expected. As such, these drug combinations could be expected to perform poorly in clinical cancer treatment. The prevalence of antagonistic RCD pathway interactions highlights the need for careful annotation of death polypharmacology in agents used in clinical combinations. Agents that induce death polypharmacology are at risk of showing varied clinical outcomes in drug combination depending on what pathway is selected.

For instance, our study found that MNNG can induce either apoptosis or parthanatos, depending on the dose. Parthanatotic doses of MNNG would result in less death than expected when paired with an apoptotic agent. This decreased cell death would likely result in worse clinical outcomes for cancer patients. Instead, apoptotic doses of MNNG should be paired with an apoptotic agent. This would likely improve clinical outcomes. As such, cataloging RCD pathway interactions and instances of death polypharmacology will allow for better clinical combination therapy design.

3.2 Implications for Combinations of DNA Damaging Agents and PARP Inhibitors

Our study relies on the use of Rucaparib, a PARP-1 inhibitor, to characterize the DNA alkylating agent, MNNG. PARP inhibitors are frequently used as single-agent therapies to treat ovarian cancers and breast cancers.^{101,102,103,104,105,106,107,108,109} Since PARP-1 is involved in DNA damage repair, PARP inhibitors reduce a cell's ability to repair DNA damage. As such, DNA damaging agents are an obvious drug combination partner for PARP inhibitors. Accordingly, early clinical studies tested PARP inhibitors in combination with DNA damaging agents.^{101,110,111,112} However, these combinations were too toxic for clinical use. In spite of these issues, combinations of DNA damaging agents and PARP inhibitors are still attractive clinical strategies. New combination strategies are currently being tested to limit toxicity.^{101,113,114}

Our study combined a PARP inhibitor, Rucaparib, with a DNA damaging agent, MNNG. We found that death induced by parthanatotic doses of MNNG was blocked by Rucaparib treatment. Conversely, we found that death induced by apoptotic doses of MNNG was enhanced by Rucaparib treatment. This finding has important implications for potential combinations of PARP inhibitors with DNA damaging agents.

Our study shows that DNA damaging agent RCD pathway induction can guide rational combination design with PARP inhibitors. Specifically, DNA damaging

agents that induce apoptosis will result in more death when combined with PARP inhibitors. This could result in improved clinical drug efficacy. However, this could also result in increased toxicities. Conversely, DNA damaging agents that induce parthanatos will result in less death when combined with PARP inhibitors. This could result in decreased clinical drug efficacy.

Overall, this finding highlights the importance of characterizing and studying the effect of RCD on clinical treatment outcomes for combination therapies. Moreover, it again highlights the importance of dose-dependent death polypharmacology and dose selection in guiding combinations. For combination with PARP inhibitors, DNA damaging agent dose-dependent death polypharmacology could alter expected clinical outcomes. Thus, for PARP inhibitor combinations, DNA damaging agent death pathway engagement needs to be tested across dose. Optimized drug death pathway selection will result in optimized combination therapies.

3.3 Importance of Kinetics for Capturing Death Polypharmacology

Our study reveals that MNNG induces a form of dose-dependent death polypharmacology. Intermediate doses of MMNG induce parthanatotic death.

However, high doses of MNNG switch to induction of apoptotic death. As previously highlighted, this dose-dependent death polypharmacology is important to consider for clinical therapy and drug combination outcomes. Although MNNG is not a clinical compound, other drugs utilized in the clinic likely exhibit the same phenomenon. For this reason, it is necessary to characterize what drugs are capable of inducing dose-dependent death polypharmacology.

In this study, we relied upon the use of death kinetics to capture the phenomenon of dose-dependent death polypharmacology. Specifically, we looked at MNNG lethal fraction (LF) kinetics. LF is the comparison of the number of dead drug-treated cells to the number of total (live and dead) drug-treated cells. LF data is plotted for a single dose across time and fit to a lag-exponential model of cell death (LED).⁷⁵ The resulting plot allows for inference of death kinetic features such as death onset time and death rate. Comparing changes in these features across dose allowed us to capture the MNNG dose-dependent death polypharmacology phenomenon. We found that the parthanatotic doses of MNNG induce death with a faster onset time, but slower rate. However, the apoptotic doses of MNNG induce death with a slower onset time, but faster rate. This change in death onset time and death rate led us to conclude that a death mechanism switch had likely occurred.

Traditional pharmacometrics, such as RV dose-response, did not reveal MNNG dose-dependent death polypharmacology. Since most drug studies rely on RV, it is unsurprising that this phenomenon has not been captured before. Similarly, FV

metrics only hinted at a death mechanism switch when comparing dose-response curves of MNNG plus and minus parthanatotic inhibitor, Rucaparib. Moreover, the assay endpoint changed whether this phenomenon was observable by FV. This highlights that kinetic death assays, like FLICK and STACK, are required to observe features of death polypharmacology. As such, kinetic death data should be included when evaluating drug response. This is especially true for drugs that will be utilized in clinical combination therapies.

3.4 Improving Mechanistic Insight for the Parthanatos Pathway

Parthanatos is an inflammatory form of RCD dependent upon poly (ADP-ribose) polymerase 1 (PARP-1) hyper-activation.^{2,3,52,53,54,55} Because it is caspase-independent, parthanatos is distinct from apoptosis. Due to this distinction, parthanatos is a potentially attractive target for apoptosis-resistant forms of cancer.⁵¹ However, the parthanatos pathway is poorly defined. This makes it challenging to design novel and specific parthanatotic agents.

While studies agree that parthanatos involves PARP-1 and PAR production,^{51,54,55,56,57,58,59} the remaining pathway steps are unclear. Some studies suggest the involvement of apoptosis-inducing factor (AIF).⁵⁶ However, other

studies have found that AIF is not essential for parthanatos execution.^{61,62,63} This uncertainty highlights the need for additional studies into the mechanism of parthanatos. Specifically, additional parthanatos pathway clarity is required to develop novel therapies to target cancer.

Our study offers new insight into the parthanatotic pathway. Foremost, our study found that MNNG can induce either parthanatos or apoptosis. However, MNNG has frequently been used to study parthanatotic death across a wide range of doses.^{53,54,56,60,83,84,85} As such, previous studies of parthanatos could have used an apoptotic dose of MNNG. This could explain why many discrepancies exist across studies attempting to define the molecular mechanism of parthanatos.

Our study also offers insight into parthanatos pathway crosstalk with apoptosis. We found that apoptosis and parthanatos are mutually exclusive, which was also reported by our lab in another study.⁴⁹ It is already known that apoptosis can inhibit parthanatos by apoptotic executioner Caspase-3 cleavage of PARP-1.⁶⁴ However, it is unclear how parthanatos inhibits apoptosis. Our current mechanism of parthanatos does not show a clear pathway connection to apoptosis. Yet, this study, and previous work in our lab,⁴⁹ has shown that the apoptotic and parthanatotic pathways must connect.

Moreover, our study offers a new opportunity to improve our understanding of the precise molecular mechanism of parthanatos. We have found that the parthanatotic drug, MNNG, induces either growth arrest, parthanatos, or

apoptosis. The specific outcome is mediated by dose-selection. Thus, we propose a CRISPR screen of MNNG across doses. The screen design would rely on careful selection of a growth arresting dose, a parthanatotic dose, and an apoptotic dose of MNNG.

Comparing CRISPR screen hits across all three doses could serve as a powerful means of improving our current definition of parthanatos. CRISPR screen hits that appear across doses would represent non-specific MNNG effects. CRISPR screen hits that appear at a single dose would represent specific death pathway or growth arrest effects. As such, CRISPR screen hits that only appear at the parthanatotic dose of MNNG should all be related to the parthanatotic pathway. Moreover, a CRISPR screen of this design should allow for defining how parthanatos and apoptosis connect. CRISPR screen hits that sensitize cells to the apoptotic dose of MNNG could represent how parthanatos inhibits apoptosis.

The resolution of this CRISPR screen could likely be further improved by incorporating a parthanatotic inhibitor, such as Rucaparib. With this screen design, each dose of MNNG would be tested plus or minus Rucaparib. Parthanatos can only proceed in the absence of Rucaparib. Thus, comparison of the parthanatotic dose of MNNG, plus or minus Rucaparib, would allow for clear separation of parthanatos-specific CRISPR screen hits. Moreover, Rucaparib exacerbates death induced by the apoptotic dose of MNNG. Comparison of the apoptotic dose of MNNG, plus or minus Rucaparib, would allow us to elucidate the mechanism of this Rucaparib/MNNG drug synergy. Uncovering this mechanism of synergy could

have important implications for drug combinations of PARP-inhibitors and DNA damaging agents.

To-date, only a few CRISPR screens of parthanatos or MNNG have been performed. One CRISPR screen from Olivieri *et al* focused on characterizing the DNA damage effects of a non-lethal dose of MNNG.¹¹⁵ Thus, this study offered no insight on parthanatos. Conversely, another CRISPR screen from Yang *et al* focused on characterizing a lethal, parthanatotic dose of MNNG.⁸³ However, this CRISPR screen returned very few hits. Moreover, this CRISPR screen failed to find key genetic determinants of parthanatos, such as PARP-1. As such, this highlights that traditional CRISPR screen designs have limited resolution for resolving the mechanism of parthanatos. Therefore, it is necessary to explore alternate CRISPR screen designs to elucidate the parthanatotic pathway. Our study highlights that conducting a CRISPR screen across multiple doses of MNNG, plus or minus Rucaparib, could improve our ability to find key genetic determinants of parthanatos.

BIBLIOGRAPHY

1. Wong RSY. Apoptosis in cancer: from pathogenesis to treatment. *Journal of Experimental & Clinical Cancer Research*. **30:87**, 1-14 (2011).
2. Galluzzi L, Vitale I, *et al.* Molecular mechanisms of cell death: recommendations of the Nomenclature Committee on Cell Death 2018. *Cell Death Differ*. **25**, 486-541 (2018).
3. Galluzzi L, Vitale I, *et al.* Molecular definitions of cell death subroutines: recommendations of the Nomenclature Committee on Cell Death 2012. *Cell Death Differ*. **19**, 107-120 (2012).
4. Nunez G, London L, Hockenbery D, Alexander M, McKearn JP, and Korsmeyer SJ. Deregulated Bcl-2 gene expression selectively prolongs survival of growth factor-deprived hemopoietic cell lines. *J Immunol*. **144**, 3602-3610 (1990).
5. Bleicken S, Jeschke G, Stegmüller C, Salvador-Gallego R, García-Sáez AJ, and Bordignon E. Structural model of active Bax at the membrane. *Mol Cell*. **56(4)**, 496-505 (2014).
6. Salvador-Gallego R, Mund M, Cosentino K, Schneider J, Unsay J, Schraermeyer U, Engelhardt J, Ries J, and García-Sáez AJ. Bax assembly into rings and arcs in apoptotic mitochondria linked to membrane pores. *EMBO J*. **35(4)**, 389-401 (2016).
7. Grobe L, Wurm CA, Brüser C, Neumann D, Jans DC, and Jakobs S. Bax assembles into large ring-like structures remodeling the mitochondria outer membrane in apoptosis. *EMBO J*. **34(4)**, 402-413 (2016).
8. Aluvila S, Mandal T, Hustedt E, Fajer P, Choe JY, and Oh KJ. Organization of the mitochondrial apoptotic BAK pore: oligomerization of the BAK homodimers. *J Bio Chem*. **289(5)**, 2537-2551 (2014).
9. Liu X, Kim CN, Yang J, Jemmerson R, and Wang X. Induction of apoptotic program in cell-free extracts: requirement for dATP and Cytochrome c. *Cell*. **86(1)**, 147-157 (1996).

10. Li K, Li Y, Shelton JM, Richardson JA, Spencer E, Chen ZJ, Wang X, and Williams RS. Cytochrome c deficiency causes embryonic lethality and attenuates stress-induced apoptosis. *Cell*. **101(4)**, 389-399 (2000).
11. Li P, Nijhawan D, Budihardjo I, Srinivasula SM, Ahmed M, Alnemri ES, and Wang X. Cytochrome c and dADP-dependent formation of Apaf-1/caspase-9 complex initiates an apoptotic protease cascade. *Cell*. **91(4)**, 479-489 (1997).
12. Chai J, Du C, Wu JW, Kyin S, Wang X, and Shi Y. Structural and biochemical basis of apoptotic activation by Smac/DIABLO. *Nature*. **406(6798)**, 855-862 (2000).
13. Verhagen AM, Ekert PG, Pakusch M, Silke J, Connolly LM, Reid GE, Moritz RL, Simpson RJ, and Vaux DL. Identification of DIABLO, a mammalian protein that promotes apoptosis by binding to and antagonizing IAP proteins. *Cell*. **102(1)**, 43-53 (2000).
14. Du C, Fang M, Li Y, Li L, and Wang X. Smac, a mitochondrial protein that promotes cytochrome c-dependent caspase activation by eliminating IAP inhibition. *Cell*. **102(1)**, 33-42 (2000).
15. Eckelman BP and Salvesen GS. The human anti-apoptotic proteins cIAP1 and cIAP2 bind but do not inhibit caspases. *J Biol Chem*. **(281)**, 3254-3260 (2006).
16. Naito M, Nagashima K, Mashima T, and Tsuruo T. Phosphatidylserine externalization is a downstream event of interleukin-1 beta-converting enzyme family protease activation during apoptosis. *Blood*. **89(6)**, 2060-2066 (1997).
17. Martin SJ, Finucane DM, Amarante-Mendes GP, O'Brien GA, and Green DR. Phosphatidylserine externalization during CD95-induced apoptosis of cells and cytoplasts requires ICE/CED-3 protease activity. *J Biol Chem*. **271(46)**, 28753-28756 (1996).
18. Sebbagh M, Renvoizé C, Hamelin J, Riché N, Bertoglio J, and Bréard J. Caspase-3-mediated cleavage of ROCK I induces MLC phosphorylation and apoptotic membrane blebbing. *Nat Cell Bio*. **3(4)**, 346-352 (2001).
19. Coleman ML, Sahai EA, Yeo M, Bosch M, Dewar A, and Olson MF. Membrane blebbing during apoptosis results from caspase-mediated activation of ROCK I. *Nat Cell Bio*. **3(4)**, 339-345 (2001).

20. Fernald K and Kurokawa M. Evading apoptosis in cancer. *Trends in Cell Biol.* **23(12)**, 620-633 (2013).
21. Hanahan D and Weinberg RA. Hallmarks of cancer: the next generation. *Cell.* **144**, 646-674 (2011).
22. Sharma A, Boise LH, and Shanmugam M. Cancer metabolism and the evasion of apoptotic cell death. *Cancers.* **11**, 1144 (2019).
23. Kaufmann SH, Karp JE, Svingen PA, Krajewski S, Burke PJ, Gore SD, and Reed JC. Elevated expression of apoptotic regulator Mcl-1 at the time of leukemic relapse. *Blood.* **91(3)**, 991-1000 (1998).
24. Taniai M, Grambihler A, Higuchi H, Werneberg N, Bronk SF, Farrugia DJ, Kaufmann SH, and Gores GJ. MCL-1 mediates tumor necrosis factor-related apoptosis-inducing ligand resistance in human cholangiocarcinoma cells. *Cancer Res.* **64(10)**, 3517-3524 (2004).
25. Wuillème-Toumi S, Robillard N, Gomez P, Moreau P, Le Gouill S, Avet-Loiseau H, Harousseau JL, Amiot M, and Bataille R. MCL-1 is overexpressed in multiple myeloma and associated with relapse and shorter survival. *Leukemia.* **19(7)**, 1248-1252 (2005).
26. Bakhshi A, Jensen JP, Goldman P, Wright JJ, McBride OW, Epstein AL, and Korsmeyer SJ. Cloning chromosomal breakpoint of t(14;18) human lymphomas: clustering around JH on chromosome 14 and near a transcriptional unit on 18. *Cell.* **41(3)**, 899-906 (1985).
27. Cleary M and Sklar J. Nucleotide sequence of a t(14;18) chromosomal breakpoint in follicular lymphoma and demonstration of a breakpoint-cluster region near a transcriptionally active locus on chromosome 18. *PNAS.* **82(21)**, 7439-7443 (1985).
28. Tsujimoto Y, Gorham J, Cossman J, Jaffe E, and Croce CM. The t(14;18) chromosome translocations involved in B-cell neoplasms results from mistakes in VDJ joining. *Science.* **229(4720)**, 1390-1393 (1985).
29. Tonon G, Wong K, *et al.* High-resolution genomic profiles of human lung cancer. *PNAS.* **102(27)**, 9625-9630 (2005).
30. Smith LT, Mayerson J, Nowak NJ, Suster D, Mohammed N, Long S, Auer H, Jones S, McKeegan C, Young G, Bos G, Plass C, and Morrison C. 20q11.1 amplification in giant-cell tumor of bone: Array CGH, FISH, and association with outcome. *Genes Chromosome Cancer.* **45(10)**, 957-966 (2006).

31. Beroukhim R, Mermel C, *et al.* The landscape of somatic copy-number alteration across human cancers. *Nature*. **463**, 899-905 (2010).
32. Kendall J, Liu Q, Bakleh A, Krasnitz A, Nguyen KCQ, Lakshmi B, Gerard WL, Powers S, and Mu D. Oncogenic cooperation and coamplification of developmental transcription factor genes in lung cancer. *PNAS*. **104(42)**, 16663-16668 (2007).
33. Kurokawa M, Kim J, *et al.* A network of substrates of the E3 ubiquitin ligases MDM2 and HUWE1 control apoptosis independently of P53. *Sci Signal*. **6(274)**, ra32 (2013).
34. Ding Q, He X, Xia W, Hsu J, Chen C, Li L, Lee D, Yang J, Xie X, Liu J, and Hung M. Myeloid cell leukemia-1 inversely correlates with glycogen synthase kinase-3 β activity and associates with poor prognosis in human breast cancer. *Cancer Res*. **67(10)**, 4564-4571 (2007).
35. Inuzuka H, Shaik S, *et al.* SCF^{FBW7} regulates cellular apoptosis by targeting MCL1 for ubiquitylation and destruction. *Nature*. **471**, 104-109 (2011).
36. Wertz IE, Kusam S, *et al.* Sensitivity to antitubulin chemotherapeutics is regulated by MCL1 and FBW7. *Nature*. **471**, 110-114 (2011).
37. Soengas MS, Capodiceci P, Polsky D, Mora J, Esteller M, Optiz-Araya X, McCombie R, Herman JG, Gerald WL, Lazebnik YA, Cordon-Cardó C, and Lowe SW.
38. Dai DL, Martinka M, Bush JA, and Li G. Reduced Apaf1 expression in human cutaneous melanomas. *Br. J. Cancer*. **91**, 1089-1095 (2004).
39. Fujimoto A, Takeuchi H, Taback B, Hsueh EC, Elashoff D, Morton L, and Hoon DBS. Allelic imbalance of 12q22-23 associated with APAF1 locus correlates with poor disease outcome in cutaneous melanoma. *Cancer Res*. **64(6)**, 2245-2250 (2004).
40. Umetani N, Fujimoto A, Takeuchi H, Shinozaki M, Bilchik AJ, and Hoon DSB. Allelic imbalance of APAF-1 locus at 12q23 is related to progression of colorectal cancer. *Oncogene*. **23(50)**, 8292-8300 (2004).
41. Zlobec I, Mino P, Baker K, Haegert D, Khetani K, Tornillo L, Terracciano L, Jass JR, and Lugli A. Loss of APAF-1 expression is associated with tumor progression and adverse prognosis in colorectal cancer. *Eur J Cancer*. **43(6)**, 1101-1107 (2007).

42. Wang H, Bai H, Li Y, Sun J, and Wang X. Rationales for expression and altered expression of apoptotic protease activating factor-1 gene in gastric cancer. *World J Gastroenterol.* **13(38)**, 5060-5064 (2007).
43. Christoph F, Hinz S, Kempkensteffen C, Weikert S, Krause H, Schostak M, Schrader M, and Miller K. A gene expression profile of tumor suppressor genes commonly methylated in bladder cancer. *J Cancer Res Clin Oncol.* **133(6)**, 343-349 (2006).
44. Hinz S, Kempkensteffen C, Weikert S, Schostak M, Schrader M, Miller K, and Christoph F. EZH2 polycomb transcriptional repressor expression correlates with methylation of the APAF-1 gene in superficial transitional cell carcinoma of the bladder. *Tumour Biol.* **28(3)**, 151-157 (2007).
45. Agrawal SG, Liu F, Wiseman C, Shirali S, Liu H, Lillington D, Du M, Syndercombe-Court D, Newland AC, Gribben JG, and Jia L. *Blood.* **111(5)**, 2790-2796 (2008).
46. Shen XG, Li Y, Wang L, Zhou B, Zu B, Jiang X, Zhou ZG, and Sun XF. Downregulation of caspase-9 is a frequent event in patients with stage II colorectal cancer and correlates with poor clinical outcome. *Colorectal Dis.* **12(12)**, 1213-1218 (2010).
47. Devarajan E, Sahin AA, Chen JS, Krishnamurty RR, Aggarawal N, Brun AM, Sapino A, Zhang F, Sharma D, Yang XH, Tora AD, and Mehta K. Downregulation of caspase 3 in breast cancer: a possible mechanism for chemoresistance. *Oncogene*, **21(57)**, 8843-8851 (2002).
48. Fong PC, Xue WC, Ngan HYS, Chiu PM, Chan KYK, Tsao GSW, and Cheung ANY. Caspase activity is downregulated in choriocarcinoma: a cDNA array differential expression study. *J Clin Pathol.* **59(2)**, 179-183 (2006).
49. Richards R, Schwartz HR, Honeywell ME, Stewart MS, Cruz-Gordillo P, Joyce AJ, Landry BD, and Lee MJ. Drug antagonism and single-agent dominance result from differences in death kinetics. *Nat Chem Bio.* **16**, 791-800 (2020).
50. Zhang C, Liu X, Jin S, Chen Y, and Guo R. Ferroptosis in cancer therapy: a novel approach to reversing drug resistance. *Molecular Cancer.* **21**, 47 (2022).
51. Zhao N, Mao Y, Han G, Ju Q, Zhou L, Liu F, Xu Y, Zhao X. YM155 a survivin suppressant, triggers PARP-dependent cell death (parthanatos) and inhibits esophageal squamous-cell carcinoma xenografts in mice. *Oncotarget.* **6(21)**, 18845-18459 (2015).

52. Yu S, Wang H, Poitras MF, Coombs C, Bowers WJ, Federoff WJ, Poirier GG, Dawson TM, and Dawson VL. Mediation of poly(ADP-ribose) polymerase-1 dependent cell death by apoptosis-inducing factor. *Science*. **297**, 259-263 (2002).
53. Yu S, Andrabi SA, Wang H, Kim NS, Poirier GG, Dawson TM, and Dawson VL. Apoptosis-inducing factor mediates poly(ADP-ribose) (PAR) polymer-induced cell death. *PNAS*. **103(48)**, 18314-18319 (2006).
54. Wang Y, Dawson VL, and Dawson TM. Poly(ADP-ribose) signals to mitochondrial AIF: a key event in parthanatos. *Exp Neurol*. **218**, 193-202 (2009).
55. Wang Y, Kim NS, Haince J, Kang H, David KK, Andrabi S, Poirier GG, Dawson VL, and Dawson TM. Poly(ADP-ribose) (PAR) binding to apoptosis-inducing factor is critical for PAR polymerase-1-dependent cell death (parthanatos). *Sci Signal*. **4(167)**, ra20 (2012).
56. Wang Y, An R, *et al.* A nuclease that mediates cell death induced by DNA damage and poly(ADP-ribose) polymerase-1. *Science*. **354(6308)**, doi:10.1126/science.aad6872 (2016).
57. Zheng L, Wang C, Luo T, Lu B, Ma H, Zhou Z, Zhu D, Chi G, Ge P, and Luo Y. JNK activation contributes to oxidative stress-induced parthanatos in glioma cells via increase in intracellular ROS production. *Mol Neurobio*. **54**, 3492-3505 (2017).
58. Ma D, Lu B, Feng C, Wang C, Wang Y, Luo T, Feng J, Jia H, *et al.* Deoxypodophyllotoxin triggers parthanatos in glioma cells via induction of excessive ROS. *Cancer Lett*. **371**, 194-204 (2016).
59. Prokhorova EA, Egorshina AY, Zhivotovsky B, and Koepina GS. The DNA-damage response and nuclear events as regulators of nonapoptotic forms of cell death. *Oncogene*. **(39)**, 1-16 (2020).
60. Andrabi SA, Kim NS, *et al.* Poly(ADP-ribose) (PAR) polymer is a death signal. *PNAS*. **103(48)**, 18308-18313 (2006).
61. Zhang F, Xie R, Munoz FM, Lau SS, and Monks TJ. PARP-1 hyperactivation and reciprocal elevations in intracellular Ca²⁺ during ROS-induced non-apoptotic cell death. *Toxicological Sci*. **140(1)**, 118-134 (2014).
62. Jang K, Do Y, Son D, Son E, Choi J, and Kim E. AIF-independent parthanatos in the pathogenesis of dry age-related macular degeneration. *Cell Death and Disease*. **8**, e2526 (2017).

63. Regdon Z, Robaszkiewicz A, Kovács K, Rygielska Z, Hegedűs C, Bodoor K, Szabó E, and Virág L. LPS protects macrophages from AIF-independent parthanatos by downregulation of PARP1 expression, induction of SOD2 expression, and a metabolic shift to aerobic glycolysis. *Free Radic Biol Med.* **131**, 184-196 (2019).
64. Soldani C and Scovassi A. Poly(ADP-ribose) polymerase-1 cleavage during apoptosis: an update. *Apoptosis.* **7**, 321-328 (2002).
65. Oberst A, Dillon CP, Weinlich R, McCormick LL, Fitzgerald P, Pop C, Hakem R, Salvesen GS, and Green DR. Catalytic activity of the caspase-8-FLIP_L complex inhibits RIPK3-dependent necrosis. *Nature.* **471(7338)**, 363-367 (2011).
66. Mokhtari RB, Homayouni TS, Baluch N, Morgatskaya E, Kumar S, Das B, and Yeger H. Combination therapy in cancer. *Oncotarget.* **8(23)**, 38022-38043 (2017).
67. Frantz S. Playing dirty. *Nature.* **437**, 942-943 (2005).
68. Dixon SJ, Patel DN, Welsch W, Skouta R, *et al.* Pharmacological inhibition of cysteine-glutamate exchange induces endoplasmic reticulum stress and ferroptosis. *Elife.* **3**, e02523 (2014).
69. Louandre C, *et al.* The retinoblastoma (Rb) protein regulates ferroptosis induced by sorafenib in human hepatocellular carcinoma cells. *Cancer Lett.* **356**, 971-977 (2015).
70. Lachaier E, *et al.* Sorafenib induces ferroptosis in human cancer cell lines originating from different solid tumors. *Anticancer Res.* **34**, 6417-6422 (2014).
71. Louandre C, *et al.* Iron-dependent cell death of hepatocellular carcinoma cells exposed to sorafenib. *Int J Cancer.* **133**, 1732-1742 (2013).
72. Sonntag R, Gassler N, Bangen JM, Trautwein C, and Liedtke C. Pro-apoptotic sorafenib signaling in murine hepatocytes depends on malignancy and is associated with PUMA expression *in vitro* and *in vivo*. *Cell Death and Disease.* **5**, e1030 (2014).
73. Wang S, Konorev EA, Kotamraju S, Joseph J, Kalivendi S, and Kalyanaraman B. Doxorubicin induces apoptosis in normal and tumor cells via distinctly different mechanisms. *J Biol Chem.* **279(24)**, 25535-25542 (2004).

74. Zhang T, Zhang Y, *et al.* CaMKII is a RIP3 substrate mediating ischemia- and oxidative stress-induced myocardial necroptosis. *Nature Med.* **22(2)**, 175-184 (2014).
75. Richards R, Honeywell ME, and Lee MJ. FLICK: an optimized plate reader-based assay to infer cell death kinetics. *STAR Protocols.* **2**, 100327 (2021).
76. Schwartz HR, Richards R, Fontana RE, Joyce AJ, Honeywell ME, and Lee MJ. Drug GRADE: an integrated analysis of population growth and cell death reveals drug-specific and cancer subtype-specific response profiles. *Cell Rep.* **31**, 107800 (2020).
77. Hafner M, Niepel M, Chung M, and Sorger PK. Growth rate inhibition metrics correct for confounders in measuring sensitivity to cancer drugs. *Nat Methods.* **13(6)**, 521-526 (2016).
78. Hafner M, Heiser LM, Williams EH, Niepel M, Wang NJ, Korkola JE, Gray JW, and Sorger PK. Quantification of sensitivity and resistance of breast cancer cell lines to anti-cancer drugs using GR metrics. *Sci Data.* **4**, 170166 (2017).
79. Forcina GC, Conlon M, Wells A, Cao JW, and Dixon SJ. Systematic quantification of population cell death kinetics in mammalian cells. *Cell Systems.* **4**, 600-610 (2017).
80. Hammill AK, Uhr JW, and Scheuermann RH. Annexin V staining due to loss of membrane asymmetry can be reversible and precede commitment to apoptotic death. *Exp Cell Res.* **251**, 16-21 (1999).
81. Murai J, Huang SN, Das BB, Renaud A, Zhang Y, Doroshow JH, Ji J, Takeda S, and Pommier Y. Differential trapping of PARP1 and PARP2 by clinical PARP inhibitors. *Cancer Res.* **72(21)**, 5588-5599 (2012).
82. Murai J, Huang SN, Renaud A, Zhang Y, Ji J, Takeda S, Morris J, Teicher B, Doroshow JH, and Pommier Y. Stereospecific PARP trapping by BMN 673 and comparison with Olaparib and Rucaparib. *Mol Cancer Ther.* **13(2)**, 433-443 (2014).
83. Yang M, Wang C, Zhou M, Bao L, Wang Y, Kumar A, Zing C, Luo W, and Wang Y. KDM6B promotes PARthanatos via suppression of O⁶-methylguanine DNA methyltransferase repair and sustained checkpoint response. *Nuc Acids Res.* **50(11)**, 6313-6331 (2022).
84. Murata MM, Kong X, Moncada E, Chen Y, Imamura H, Wang P, Berns MW, Yokomori K, and Digman MA. *MBoC.* **30**, 2584-2597 (2019).

85. Gagne J, Isabelle M, Lo KS, Bourassa S, Hendzel MJ, Dawson VL, Dawson TM, and Poirier GG. Proteome-wide identification of poly(ADP-ribose) binding proteins and poly(ADP-ribose)-associated protein complexes. *Nuc Acids Res.* **36(22)**, 6959-6976 (2008).
86. Slamenová D, Gábelová A, Ruzeková L, Chalupa I, Horváthová E, Farkasová T, Bozsakyová E, and Stětina R. Detection of MNNG-induced DNA lesions in mammalian cells; validation of comet assay against DNA unwinding technique, alkaline elution of DNA and chromosomal aberrations. *Mut Res.* **383**, 243-252 (1997).
87. Giglia-Mari G, Zotter A, and Vermeulen W. DNA damage response. *Cold Spring Harb Perspect Biol.* **3**, a000745 (2011).
88. El-Khamisy SF, Katyal S, Patel P, Ju L, McKinnon PJ, and Caldecott KW. Synergistic decrease of DNA single-strand break repair rates in mouse neural cells lacking both Tdp1 and aprataxin. *DNA Repair.* **8**, 760-766 (2009).
89. Gueven N, Necherel OJ, Kijas AW, Chen P, Howe O, Rudolph JH, Gatti R, Date H, Onodera O, Taucher-Scholz G, *et al.* Aprataxin, a novel protein that protects against genotoxic stress. *Hum Mol Gen.* **13**, 1081-1093 (2004).
90. McGrail DJ, Garnett J, *et al.* Proteome instability is a therapeutic vulnerability in mismatch repair-deficient cancer. *Cancer Cell.* **37**, 371-386 (2020).
91. Peng M, Xie J, Ucher A, Stavnezer J, and Cantor SB. Crosstalk between BRCA-Fanconi anemia and mismatch repair pathways prevent MSH2-dependent aberrant DNA damage responses. *EMBO.* **33(15)**, 1698-1712 (2014).
92. Gupta D, Lin B, Cowan A, and Heinen CD. ATR-Chk1 activation mitigates replication stress caused by mismatch repair-dependent processing of DNA damage. *PNAS.* **115(7)**, 1523-1528 (2018).
93. Martin JH and Dimmitt S. The rationale of dose-response curves in selecting cancer drug dosing. *BJCP.* **85**, 2198-2204 (2019).
94. Skipper HE, Schabel FR Jr., and Wilcox WS. Experimental evaluation of potential anticancer agents. XII. On the criteria and kinetics associated with "curability" of experimental leukaemia. *Cancer Chemother Rep.* **35**, 1-111 (1964).
95. Frei E, Teicher BA, Holden SA, Cathcart KNS, and Wang Y. Preclinical studies and clinical correlation of the effect of alkylating dose. *Cancer Res.* **48(22)**, 6417-6423 (1988).

96. Frei E and Canellos G. Dose: a critical factor in cancer chemotherapy. *Am J Med.* **69(4)**, 585-594 (1980).
97. Wilking N, Lidbrink E, Wilkund T, *et al.* Long-term follow-up of the SBG 9401 study comparing tailored FEC-based therapy versus marrow-supported high-dose therapy. *Ann Oncol.* **18(4)**, 694-700 (2007).
98. Stadtmauer EA, O'Neill A, Goldstein LJ, *et al.* Conventional-dose chemotherapy compared with high-dose chemotherapy plus autologous hematopoietic stem cell transplantation for metastatic breast cancer. *New Engl J Med.* **342(15)**, 1069-1076 (2000).
99. Peters WP, Rosner GL, Vredenburgh JJ, *et al.* Prospective, randomized comparison of high-dose chemotherapy with stem-cell support versus intermediate-dose chemotherapy after surgery and adjuvant chemotherapy in women with high-risk primary breast cancer: a report of CALGB 9082, SWOG 9114, and NCIC MA-13. *J Clin Oncol.* **23(10)**, 2191-2200 (2005).
100. Chapman PB, Robert C, Larkin J, *et al.* Vemurafenib in patients with BRAF^{V600} mutation-positive metastatic melanoma: final overall survival results of the randomized BRIM-3 study. *Ann Oncol.* **28(10)**, 2581–2587 (2017).
101. Yap TA, Plummer R, Azad NS, and Helleday T. The DNA damaging revolution: PARP inhibitors and beyond. ASCO. doi://10.1200/EDBK_238473 (2019).
102. Tutt A, Robson M, Garber JE, *et al.* Oral poly(ADP-ribose) polymerase inhibitor olaparib in patients with BRCA1 or BRCA2 mutations and advanced breast cancer: a proof-of-concept trial. *Lancet.* **376**, 235-244 (2010).
103. Drew Y, Ledermann J, Hall G, *et al.* Phase 2 multicentre trial investigating intermittent and continuous dosing schedules of the poly(ADP-ribose) polymerase inhibitor rucaparib in germline BRCA mutation carriers with advanced ovarian and breast cancer. *Br J Cancer.* **114**, e21 (2016).
104. Swisher EM, Lin KK, Oza AM, *et al.* Rucaparib in relapsed, platinum-sensitive high-grade ovarian carcinoma (ARIEL2 Part 1): an international, multicentre, open-label, phase 2 trial. *Lancet Oncol.* **18**, 75-87 (2017).

105. Ledermann J, Harter P, Gourley C, *et al.* Olaparib maintenance therapy in platinum sensitive relapsed ovarian cancer. *N Engl J Med.* **366**, 1382-1392 (2012).
106. Pujade-Lauraine E, Ledermann JA, Selle F, *et al.* SOLO2/ENGOT-Ov21 Investigators. Olaparib tablets as maintenance therapy in patients with platinum-sensitive, relapsed ovarian cancer and a BRCA1/2 mutation (SOLO2/ENGOT-Ov21): a double-blind, randomised, placebo-controlled, phase 3 trial. *Lancet Oncol.* **18**, 1274-1284 (2017).
107. Kristeleit R, Shapiro GI, Burris HA, *et al.* A phase I-II study of the oral PARP inhibitor rucaparib in patients with germline BRCA1/2-mutated ovarian carcinoma or other solid tumors. *Clin Cancer Res.* **23**, 4095-4106 (2017).
108. Robson M, Im SA, Senkus E, *et al.* Olaparib for metastatic breast cancer in patients with a germline BRCA mutation. *N Engl J Med.* **377**, 523-533 (2017).
109. Turner NC, Telli ML, Rugo HS, *et al.* A phase II study of talazoparib after platinum or cytotoxic nonplatinum regimens in patients with advanced breast cancer and germline BRCA1/2 mutations (ABRAZO). *Clin Cancer Res.* Epub (2018).
110. Plummer ER, Middleton MR, Wilson R, *et al.* First in human phase I trial of the PARP inhibitor AG-014699 with temozolomide (TMZ) in patients (pts) with advanced solid tumors. *J Clin Oncol.* **23(suppl)**, 3065 (2005).
111. Plummer R, Lorigan P, Steven N, *et al.* A phase II study of the potent PARP inhibitor, rucaparib (PF-01367338, AG014699), with temozolomide in patients with metastatic melanoma demonstrating evidence of chemopotential. *Cancer Chemother Pharmacol.* **71**, 1191-1199 (2013).

112. Rajan A, Carter CA, Kelly RJ, *et al.* A phase I combination study of olaparib with cisplatin and gemcitabine in adults with solid tumors. *Clin Cancer Res.* **18**, 2344-2351 (2012).
113. Powell C, Mikropoulos C, Kaye SB, *et al.* Pre-clinical and clinical evaluation of PARP inhibitors as tumour-specific radiosensitisers. *Cancer Treat Rev.* **36**, 566-575 (2010).
114. Reiss KA, Herman JM, Zahurak M, *et al.* A phase I study of veliparib (ABT-888) in combination with low-dose fractionated whole abdominal radiation therapy in patients with advanced solid malignancies and peritoneal carcinomatosis. *Clin Cancer Res.* **21**, 68-76 (2015).
115. Olivier M, Cho T, *et al.* A genetic map of the human response to DNA damage in human cells. *Cell.* **182**, 1-16 (2020).